AGU PUBLICATIONS

Geochemistry, Geophysics, Geosystems

REVIEW ARTICLE
10.1002/2016GC006334

Special Section:
FRONTIERS IN GEOSYSTEMS: Deep Earth - Surface Interactions

Key Points:
- Mantle circulation controls the geodynamo through core heat loss
- Mantle circulation models predict heterogeneous core-mantle boundary heat flux
- The inner core is young because core heat loss is high

Correspondence to:
P. Olson,
olson@jhu.edu

Citation:
Olson, P. (2016), Mantle control of the geodynamo: Consequences of top-down regulation, *Geochem. Geophys. Geosyst.*, *17*, 1935–1956, doi:10.1002/2016GC006334.

Received 29 FEB 2016
Accepted 19 APR 2016
Accepted article online 25 APR 2016
Published online 29 MAY 2016

Mantle control of the geodynamo: Consequences of top-down regulation

Peter Olson[1]

[1]Department of Earth and Planetary Sciences, Johns Hopkins University, Baltimore, Maryland, USA

Abstract The mantle global circulation, including deep subduction and lower mantle superplumes, exerts first-order controls on the evolution of the core, the history of the geodynamo, and the structure of the geomagnetic field. Mantle global circulation models that include realistic plate motions, deep subduction, and compositional heterogeneity similar to the observed large low seismic velocity provinces in the lower mantle predict that the present-day global average heat flux at the core-mantle boundary (CMB) exceeds 85 mW m^{-2}. This is sufficient to drive the present-day geodynamo by thermochemical convection and implies a very young inner core, with inner core nucleation between 400 and 1100 Ma. The mantle global circulation also generates spatially heterogeneous heat flux at the CMB, with peak-to-peak lateral variations exceeding 100 mW m^{-2}. Such extreme lateral variability in CMB heat flux, in conjunction with the high thermal conductivity of the core, implies that the liquid outer core is thermally unstable beneath the high seismic velocity regions in the lower mantle but thermally stable beneath the large low seismic velocity provinces. Numerical dynamo simulations show how this pattern of heterogeneous boundary heat flux affects flow in the outer core, producing localized circulation patterns beneath the CMB tied to the mantle heterogeneity and long-lived deviations from axial symmetry in the geomagnetic field.

1. Introduction

Two gigantic heat engines are active inside the Earth. One is the convective heat engine operating inside the mantle that drives plate motions, continental drift, and controls most of the tectonic processes we observe at the surface. In this paper, we refer to this heat engine as the mantle global circulation. The other engine operates mainly inside the core and produces flow in the liquid outer core, primarily through differentiation processes connected to the growth of the solid inner core, but also through thermal buoyancy. We call this engine the geodynamo, because it sustains the main geomagnetic field. Both of these engines have operated over much of Earth history. Petrologic evidence indicates that plate tectonics and global mantle circulation have been present for at least 3×10^9 years [*Shirey and Richardson*, 2011]. Similarly, paleomagnetic evidence indicates that the geomagnetic magnetic field has been present for at least 3.4×10^9 years [*Tarduno et al.*, 2010] and perhaps as long as 4.2×10^9 years [*Tarduno et al.*, 2015a] or more.

Although the physical properties of the mantle and core are vastly different, these two giant engines are nevertheless coupled. They interact with each other in a variety of ways, spanning an enormous range of time scales, and inducing a wide spectrum of responses. The locus of their interaction is the region on either side of the core-mantle boundary, denoted hereafter by CMB. The shortest known time scales in their interaction that produce irreversible changes involve precession, nutation, and tides. Precession induces a small amplitude, nearly diurnal motion of the mantle relative to the core, that potentially can be transmitted through the entire liquid outer core by inertial waves [*Tilgner*, 2015]. Nutation also consists of periodic variations in the direction of Earth's rotation axis forced by solar and lunar tides, and it also produces relative rotations between the mantle and the core, again at nearly diurnal frequencies [*Herring et al.*, 2002]. Evidence of irreversible interaction is the observed phase lag between the nutation and its astronomical forcing that has been attributed to Ohmic heating in the electrically conducting lower mantle [*Buffett*, 1992] and viscous dissipation in the liquid outer core [*Deleplace and Cardin*, 2006]. Tidal energy is dissipated in the CMB region through these same processes.

On somewhat longer time scales, there are electro-mechanical interactions, which transfer angular momentum between the core and the mantle, including those responsible for the observed variations in the length

of day (lod), for which the multidecadal lod variability (about 60 years) has received most attention. Proposed mechanisms for the cause of the angular momentum transfer include pressure forces acting on core-mantle boundary topography [*Jault and LeMouel*, 1989; *Calkins et al*., 2012], electromagnetic and gravitational torques that yield inner core-mantle coupling [*Mound and Buffett*, 2005a], and torsional oscillations in the fluid outer core [*Dumberry and Bloxham*, 2004; *Mound and Buffett*, 2005a, 2005b]. Torsional oscillations have also been implicated in the observed 6 year lod variations [*Gillet et al*., 2010].

The longest time scale interactions involve the transfer of heat and mass across the CMB. Mass transfer likely dominated this interaction during Earth's formation, when the core segregated from the mantle in response to giant impact events, primarily within the first 50–100 Myr of Earth history [*Rubie et al*., 2011; *Nakajima and Stevenson*, 2015]. Traditionally, it is assumed that, following the last giant impact, the core has been in near-chemical isolation from the mantle. Now there are reasons to doubt that assumption. Petrological and geochemical evidence supports the existence of some mass transport in both directions across the CMB (see reviews by *Jeanloz* [1990] and *Brandon and Walker* [2005]). However, it has proven extremely difficult to quantify chemical transfer rates between the core and mantle, much less demonstrate that such transfers are significant in the Earth system at the present day. But in the distant past they may have played more important roles, because cooling tends to reduce the solubility of constituents dissolved in iron and the bulk composition of the liquid core may have changed due to temperature-induced precipitation. For example, *Buffett et al*. [2000] proposed that sediments precipitated from the core accumulate on the underside of the CMB, and more recently *O'Rourke and Stevenson* [2016] proposed magnesium precipitation from the core might have served as a dynamo mechanism before the solid inner core nucleated.

The interaction between the core and mantle that has the most pervasive effect on both engines is thermal, specifically, the transfer of heat from the core to the mantle. Calculations of the evolution of the core and the mantle indicate that the core has surrendered $2-3\times10^{30}$ Joules of heat to the mantle [*Driscoll and Bercovici*, 2014; *Davies*, 2015]. Considerations of the present-day energy balance in the core indicate that the core is now surrendering heat to the mantle at a rate of 10–16 TW (TW $= 10^{12}$ Watts) [*Wu et al*., 2011; *Gomi and Hirose*, 2015; *Nimmo*, 2015; *Gubbins et al*., 2015], representing 20–40% of the total heat transferred by the mantle [*Jaupart et al*., 2007]. In order to maintain this heat flow, the mantle global circulation extends from surface to the CMB, drawing heat directly off the CMB in places, and in other places, collecting the lower mantle heterogeneity into immense debris piles, from which thermochemical instabilities originate. These thermochemical instabilities mature into mantle plumes, which, after traversing the mantle, generate huge volumes of partial melt as they intrude the lithosphere, resulting in massive volcanic events at Large Igneous Provinces (LIPs) and long-lived volcanic activity at hot spots [*Burke and Torsvik*, 2004; *Torsvik et al*., 2006; *Burke et al*., 2008; *Burke*, 2011].

On the underside of the CMB, the core is cooled by the global mantle circulation. The temperature at the CMB, now in the range of 4000–4200 K [*Andrault et al*., 2011; *Anzellini et al*., 2013], is decreasing at a rate of 10–15 K/10^8 years by virtue of heat loss to the mantle. Consequently, the temperature near the center of the Earth long ago fell below the liquidus of the core material, initiating the freezing of the solid inner core. In order to solidify the core to its present size (1220 km radius), the core must have lost $2.5-3\times10^{29}$ Joules of heat to the mantle. The time since the solid inner core nucleated is therefore a time-integrated measure of both the cooling rate of the core and the strength of the thermal coupling between the two giant engines.

What do the mantle and core get from this thermal interaction, and what are the effects on the surface environment? From the mantle perspective, the core provides basal heating, the most dramatic products of this basal heating being mantle plumes. Through formation of LIPs and hot spot volcanism, mantle plumes contribute material for new oceanic and continental crust, and they release volatiles such as CO_2 and SO_2 into the surface environment. There are close temporal connections between some large igneous provinces and major mass extinction events [*Courtillot and Renne*, 2003] implicating mantle plumes as one of the drivers for biosphere evolution.

From the core's perspective, thermal interaction with the mantle is even more important. Indeed, for the geodynamo, this interaction may be existential. Were it not for the heat flow at the CMB provided by the mantle circulation, the outer core would probably be strongly stratified, the geodynamo would likely have ceased to operate long ago, and the surface environment would lack its magnetic shield. Particularly

important in this regard is deep subduction, whereby relatively cold remnants of lithospheric slabs are brought into close proximity with the CMB, producing elevated heat flow and anomalous core cooling at those regions. This cooling is transmitted by the circulation in the outer core down to the inner core boundary, where it results in the solidification of the inner core. Solidification results in the partitioning of some lighter elements from the inner core solid to the fluid outer core. Concentrations of light elements locally reduce the density of the outer core fluid, providing the major source of buoyancy for convection in the outer core that drives the geodynamo. Although solidification of the inner core with light element partitioning at the inner core boundary is the thought to be the primary energy source for the geodynamo today, the pathway of this energy can be traced backward through the outer core and mantle, all the way to the surface, where it was first injected into the Earth system in the form of subducted ocean lithosphere. According to this perspective, the geodynamo is actually maintained by plate tectonics, telemetered deep into the core by the global mantle circulation.

How does the surface environment benefit from the geodynamo? Mainly through the maintenance of a long-lasting, strong geomagnetic shield that serves to deflect most of the solar wind, including energetic charged particles originating from the sun. Solar wind deflection minimizes the space weathering of the atmosphere by reducing the escape of ionized species. Not all of our neighbors have been so fortunate. In particular, Mars and the Moon lost their magnetic shields in the deep past, likely because their mantles failed to extract enough heat from their cores to keep dynamo processes operating [*Roberts et al*., 2009]. The situation may have even been worse on Venus, where dynamo action may never have begun [*Driscoll and Bercovici*, 2014]. Mercury may be an exception. It evidently has a weak dynamo-generated field [*Anderson et al*., 2011] and it has been proposed that planet's relatively thin mantle plays a role in its maintenance [*Ogawa*, 2016]. However, the relatively feeble external magnetic field of Mercury would not provide much of a shield for the Earth.

In this paper, I review the evidence in support of the idea that the heat flux at the CMB, which is the common denominator linking these two giant engines, is large in magnitude, has strong lateral heterogeneity, and has varied significantly over time, all consequences of the mantle global circulation. In consequence, the geomagnetic field deviates from an axial dipole in its time-averaged structure, and in addition, the inner core is the youngest major structural addition to the Earth system, probably less than 1×10^9 years in age.

The outline of this paper is as follows. First is a review of the theory and observations that point to rapid evolution of the core. The next step is to formulate simplified thermal boundary conditions at the CMB as seen individually by the mantle and core. These boundary conditions are vital elements in linking the mantle global circulation to the core dynamo. After reviewing the causes and consequences of the temporal and spatial variability of heat flux at the surface and at the CMB, I examine the response of the present-day geodynamo to the changing thermal environment of the CMB region, as revealed by numerical models of the geodynamo driven by the time variable mantle global circulation. Heat flow predictions from mantle global circulation models provide the means to evolve the core from the present-day back to the time of inner core nucleation, yielding estimates the age of the inner core and predictions of the state of the geodynamo before the inner core nucleated. Finally, some promising avenues for future progress are discussed.

2. The Rapidly Evolving Core

Our views about the core have recently changed because of the new determinations of several key properties that affect its rate of the evolution. First, the heat flow from the core to the mantle appears to be far greater than previously thought. Figure 1 shows trends in the estimates of the total CMB heat flow in terawatts (TW) versus year of publication, spanning the past 35 years. This is only a sample of an even larger set of estimates now in the literature, but it conveys an important point: our best estimates of core heat flow have progressively increased, from a few TW, to more than 10 TW, and now as high as 15 or 16 TW. Furthermore, as Figure 1 indicates, the trend toward higher core heat flow comes from a variety of approaches, including mineral physics (through upward revision in transport properties), seismic structure of the lower mantle (through interpretations of the postperovskite phase transformation), considerations of core energetics (via the entropy production needed to sustain the dynamo), and models of the mantle global circulation (from predictions of CMB heat flux).

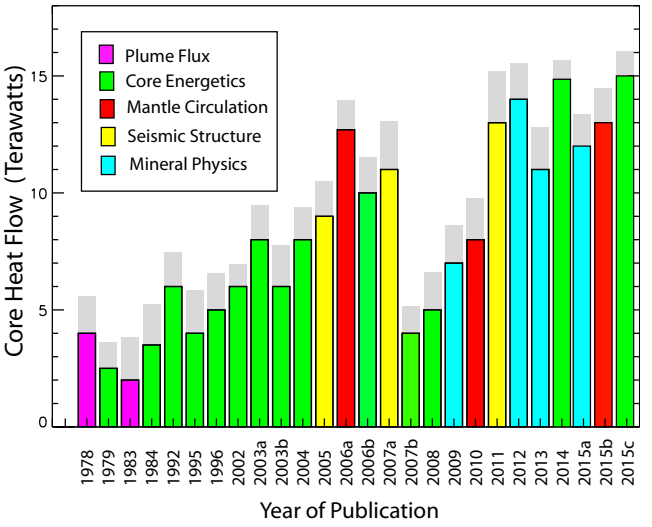

Figure 1. Estimates of the total heat flow from the present-day core versus year of publication. Solid and shaded bars denote preferred values and estimated uncertainties, respectively; bar colors indicate the main basis of the estimate. Sources: 1978: *Loper* [1978]; 1979: *Gubbins et al.* [1979]; 1983: *Stacey and Loper* [1983]; 1984: *Stacey and Loper* [1984]; 1992: *Buffett et al.* [1992]; 1995: *Lister and Buffett* [1995]; 1996: *Buffett et al.* [1996]; 2002a: *Anderson* [2002]; 2002b: *Labrosse* [2002]; 2003: *Buffett* [2003]; 2004: *Gubbins et al.* [2004]; 2005: *Hernlund et al.* [2005]; 2006a: *Zhong* [2006]; 2006b: *Lay et al.* [2006]; 2007a: *Van der Hilst et al.* [2007]; 2007b: *Stacey and Loper* [2007]; 2008: *Korenaga* [2008]; 2009: *Tateno et al.* [2009]; 2010: *Nakagawa and Tackley* [2010]; 2011: *Wu et al.* [2011]; 2012: *Pozzo et al.* [2012]; 2013: *Gomi et al.* [2013]; 2014 and 2015a: *Gubbins et al.* [2015]; 2015b: *Olson et al.* [2015]; and 2015c: *Nimmo* [2015].

The heat loss from the core translates rather directly to its rate of cooling and the rate at which the inner core grows by solidification. Consequently, in the process of underestimating core heat loss, we also overestimated the age of the inner core. This is illustrated in Figure 2, which shows estimates of the age of the inner core (hereafter denoted by ICN, the age of inner core nucleation) versus year of publication, spanning the same period of time as Figure 1. Estimates of the ICN have decreased substantially, from typically 3 or 4 $\times$ 10^9 years several decades ago to a nominal value 1 $\times$ 10^9 years or even less. If correct, this implies that the inner core is by far the youngest major structural component of the Earth system, far younger than the ocean, the continents, the oxygenated atmosphere, and the biosphere. It is even conceivable (although not likely) that the ICN was a Phanerozoic event that might be visible in the fossil record.

A third revision that has affected our perspective on the core comes from refined estimates of transport properties in the core, particularly its thermal and electrical conductivities. As Figure 3 shows, estimates of the thermal conductivity of the core have increased by a factor of at least 2 and perhaps as large as 4 over the last decade, as new theory and measurements have revealed that the electrical conductivity of iron compounds tends to rise with temperature at core pressures. A comparable increase in the thermal conductivity is also expected, based on the Wiedemann-Franz relationship for metals, implying values of the thermal conductivity in the outer core of order 100 W m^{-1} K^{-1} or higher.

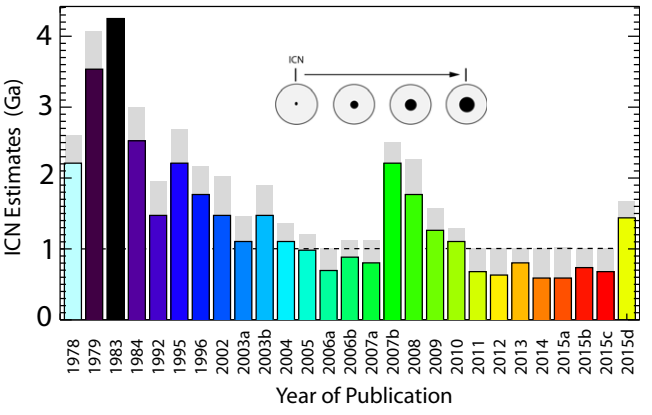

Figure 2. Estimates of the inner core age (ICN) versus year of publication. Solid and shaded bars denote preferred values and estimated uncertainties, respectively. Dashed line is 1 Ga reference age. Sources: 1978: *Loper* [1978]; 1979: *Gubbins et al.* [1979]; 1983: *Stacey and Loper* [1983]; 1984: *Stacey and Loper* [1984]; 1992: *Buffett et al.* [1992]; 1995: *Lister and Buffett* [1995]; 1996: *Buffett et al.* [1996]; 2002a: *Anderson* [2002]; 2002b: *Labrosse* [2002]; 2003: *Buffett* [2003]; 2004: *Gubbins et al.* [2004]; 2005: *Hernlund et al.* [2005]; 2006a: *Zhong* [2006]; 2006b: *Lay et al.* [2006]; 2007a: *Van der Hilst et al.* [2007]; 2007b: *Stacey and Loper* [2007]; 2008: *Korenaga* [2008]; 2009: *Tateno et al.* [2009]; 2010: *Nakagawa and Tackley* [2010]; 2011: *Wu et al.* [2011]; 2012: *Pozzo et al.* [2012]; 2013: *Gomi et al.* [2013]; 2014 and 2015a: *Gubbins et al.* [2015]; 2015b: *Olson et al.* [2015]; 2015c: *Nimmo* [2015]; and 2015d: *Biggin et al.* [2015].

The high thermal conductivity means that much of the cooling of the core is due to thermal conduction, and as a consequence, parts of the core might be thermally stratified. Figure 4 illustrates where thermal stratification may arise from the trade-off between high thermal conductivity and high core heat flow. Profiles of thermal conductivity and heat flux conducted down the core adiabat as a function of radius from *Gomi et al.* [2013] feature a strong increase in conductivity with depth, from about 90 W m^{-1} K^{-1} at the CMB to nearly 150 W

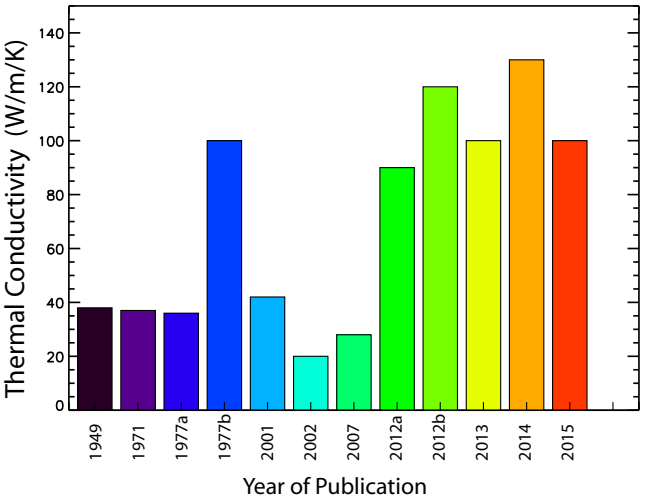

Figure 3. Estimates of the average thermal conductivity of the outer core versus year of publication. Sources: *Bullard* [1949], *Keeler* [1971], *Stacey* [1977a], *Matassov* [1977], *Stacey and Anderson* [2001], *Bi et al.* [2002], *Stacey and* Loper [2007], *Gomi et al.* [2013], *de Koker et al.* [2012], *Seagle et al.* [2013], *Pozzo et al.* [2014], and *Zhang et al.* [2015].

m^{-1} K^{-1} at the inner core boundary (ICB). The corresponding heat flux conducted down the core adiabat varies between about 40 mW m^{-2} near the ICB to nearly 70 mW m^{-2} at the CMB. Possible effects of these radial variations on the thermal state of the core are depicted in Figure 4b. Depending on the magnitude of the core heat flow, large regions of the outer core could be subadiabatic, that is, thermally stratified. In particular, thermal stratification is expected near the top of the outer core if the total core heat flow is below 11 TW, according to this model. The theoretical possibility of extensive stratification in the outer core raises multiple questions. Specifically, is there observational evidence for stable stratification in the core? And if so, what effects does it have on the evolution of the core and the operation of the geodynamo?

Observational evidence for stratification in the outer core comes primarily from two sources: anomalous seismic structure and the geomagnetic secular variation. A handful of seismic studies have identified a region below the CMB in which the seismic velocity gradients are anomalous compared to the rest of the outer core by a few percent, distributed over a region 200–300 km in thickness [*Helffrich and Kaneshima*, 2010; *Tang et al.*, 2015]. It is not known whether this anomalous region is due to thermal effects, compositional heterogeneity, or some combination of the two. Additional evidence for stable stratification below the CMB comes from the interpretation of the geomagnetic secular variation. The conventional

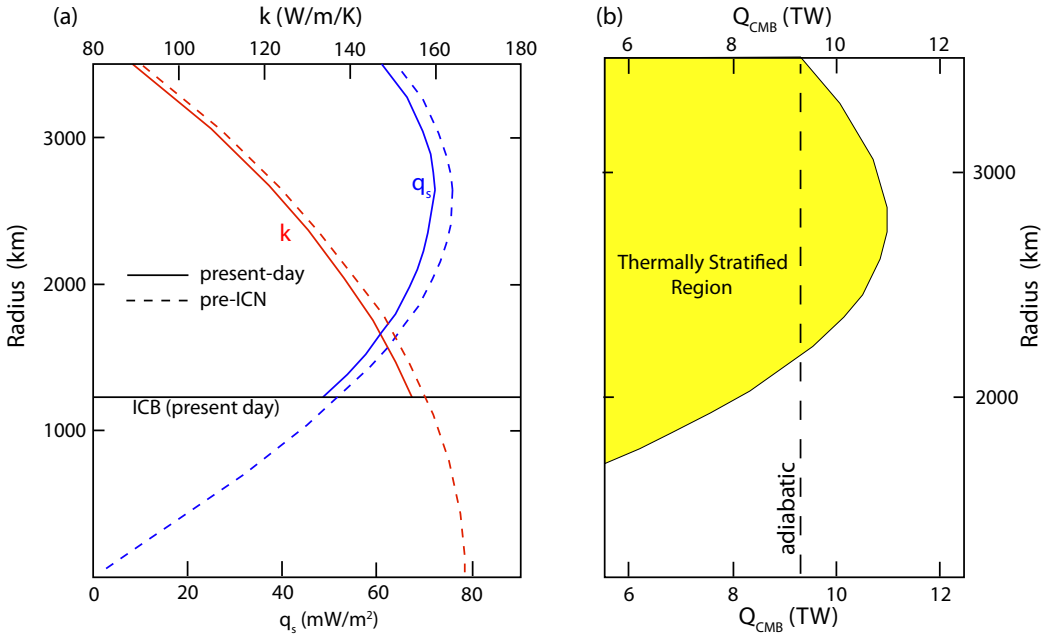

Figure 4. Thermal stratification in the core. (a) Variation of thermal conductivity k and adiabatic heat flux q_s versus radius. Dashed and solid lines denote different model assumptions. (b) Regime diagram of total heat flow at the CMB versus radius. Shading denotes depth intervals with implied thermal stratification, based on the conductivity and adiabatic heat flux profiles in Figure 4a. Vertical dashed line marks the total core heat flow that corresponds to adiabatic stratification at the CMB. Reproduced from *Gomi et al.* [2013].

interpretation of geomagnetic secular variation is that it represents transport of magnetic flux that is nearly "frozen" to the outer core fluid, and hence it acts as a tracer for the circulation beneath the CMB. Some early analyses of geomagnetic secular variation concluded that this circulation lacked upwelling components, consistent with stable stratification there [*Whaler*, 1980]. However, there are other frozen flux interpretations of the same data that come to the opposite conclusion [*Amit*, 2014]. Geomagnetic secular variation can also be produced by wave motion in the outer core. Recently, it has been proposed that geomagnetic secular variation on multidecadal time scales includes wave motions of the type called MAC waves—standing for Magnetic, Archimedian, and Coriolis. Because MAC wave propagation is sensitive to stable stratification, it is possible, in principle, to infer the strength of the stratification in the outer core from their propagation characteristics [*Buffett*, 2014].

Although there is evidence for stratification, the departures from uniform well-mixed conditions below the CMB are probably small and hence difficult to resolve quantitatively. The situation is further complicated by the fact that both thermal and compositional heterogeneity may well contribute to the stratification there [*Helffrich and Kaneshima*, 2010; *Gubbins and Davies*, 2013]. In addition, the mantle side of the CMB is among of the most heterogeneous regions inside the Earth, so the stratification below the CMB is probably not uniform. For all these reasons, the responses of the core and the geodynamo to stratification may be very complex. In this review, attention is focused on thermal stratification below the CMB, but many of the effects described here will also be present (and possibly amplified) if the stratification there is compositional.

3. Core-Mantle Thermal Interaction: Some Basics

The basics of core-mantle thermal interaction begin with the fact that the coupling is highly asymmetric. Because the viscosity of the outer core liquid [*de Wijs et al*., 1998] is more than 20 orders of magnitude less than the viscosity of the subsolidus lower mantle [*Paulson et al*., 2007], the time scale of the circulation in the outer core, measured in centuries, is orders of magnitude less than in the mantle, which is measured in tens or hundreds of millions of years. In addition, the magnitude of density anomalies due to lateral variations in temperature and composition is orders of magnitude smaller in the core than in the mantle.

To illustrate how these contrasts force the mantle and the core see each other differently in thermal interaction, consider the response of each to a thermal perturbation at the CMB on a time scale of $\sim 10^4$ years, intermediate between the circulation times in the two engines. Below the CMB, the thermal perturbation will have been mixed by the outer core circulation after 10^4 years. In terms of the heat transport equation

$$\rho C \frac{dT'}{dt} = -\nabla \cdot \mathbf{q}, \tag{1}$$

where T' denotes the temperature perturbation, ρ is density, C is specific heat, $\mathbf{q}$ is conductive heat flux, and t denotes time, exceeding the mixing time in the outer core means that $dT'/dt \simeq 0$ there. So from the perspective of the core, (1) reduces to a heat flux boundary condition at the CMB given by

$$k_c \frac{\partial T_c}{\partial r}(r_{cmb}) = -q_{cmb}, \tag{2}$$

where k is thermal conductivity, r is the radial coordinate, the c subscripts denote core properties, and q_{cmb} denotes the local mantle heat flux evaluated on the CMB, at radius r_{cmb}.

Above the CMB, in contrast, the thermal perturbation will not have been mixed by the slower mantle circulation. Instead, mixing of the thermal perturbation in the outer core generates a new (and essentially uniform) CMB temperature, T_{cmb}. From the mantle perspective, then, the appropriate thermal boundary condition at the CMB on these intermediate time scales is just

$$T_m(r_{cmb}) = T_{cmb}, \tag{3}$$

where the subscript m denotes mantle temperature.

To summarize, in their thermal interaction on intermediate time scales, the mantle sees the outer core as an isothermal reservoir, whereas the core sees the mantle as a heat sink. At the CMB, the boundary condition imposed on the outer core is the mantle heat flux, which is laterally heterogeneous, i.e., $q_{cmb}(\theta, \phi)$. The boundary condition at the CMB imposed on the mantle by the core is a uniform temperature, T_{cmb}.

Over time intervals longer than the intermediate one defined above, the only modifications to these boundary conditions that are necessary are to allow q_{cmb} and T_{cmb} to vary with time, as the two giant engines coevolve. But even here, their response is not symmetric. The shorter core mixing time ensures that, provided q_{cmb} varies on time scales long compared to the intermediate scale defined above, the response of the core can be calculated assuming equilibrium with the boundary condition at discrete epochs, that is, without considering the time dependence of the heat flux boundary condition q_{cmb} explicitly. For the mantle, in contrast, this simplification may not apply. To determine how fast the CMB temperature changes, consider the following model for core cooling:

$$\frac{dT_{cmb}}{dt} = -a\frac{Q_{cmb} - Q_{rad}}{C_c M_c}, \tag{4}$$

where Q_{cmb} is the total heat flow (area-integrated heat flux) at the CMB, Q_{rad} the radioactive heat production within the core, M_c and C_c are the core mass and specific heat, respectively, and a is a nondimensional coefficient, obtained from core evolution models. For the past 0–500 Ma during inner core growth, various core evolution scenarios [*Labrosse*, 2015; *Davies*, 2015; *Olson et al*., 2015] yield $a = 0.5 \pm 0.1$, smaller than unity because of the latent release by inner core solidification. For the present-day core, $Q_{cmb} - Q_{rad}/C_c M_c \simeq$ 0.25 K Myr^{-1}, so nominally $dT_{cmb}/dt \simeq -0.125$ K Myr^{-1}. This slow cooling rate is negligible on time scales of a few hundred million years, that is, during a single mantle overturn, but it becomes significant on time scales of billions of years that characterize the long-term evolution of the mantle [*Nakagawa and Tackley*, 2010, 2013].

Because of these asymmetries in their thermal interaction, the core can be assumed to be in thermal and compositional equilibrium with respect to the CMB heat flux on intermediate time scales and longer. However, it is not a good approximation to assume that the mantle is in thermal equilibrium, much less in compositional equilibrium, with the core. In other words, in terms of their thermal interaction, the mantle controls the core, not the other way around. This condition applies to global changes in the core—growth of the inner core, in particular—and also to changes to local structures in the core that are tied to the mantle heterogeneity.

4. CMB Heat Flux Heterogeneity

Methods for estimating present-day total core heat flow include mantle plume fluxes, the thermodynamics of the geodynamo, mineral physics-based interpretations of lowermost mantle seismic structure, and predictions from mantle global circulation models, or mantle GCMs. Figure 1 suggests that all of these approaches now predict values of the total core heat flow that correspond to a global average CMB heat flux in the range 80–100 mW m^{-2}. Assuming that the global average core heat flux lies in this range, what can be said about its spatial and temporal variability?

Indirect evidence for lateral heterogeneity of the heat flux on the CMB comes from seismology, mineral physics, and geodynamics. Seismic evidence includes variations in the double crossing of the perovskite (pv) to postperovskite (ppv) phase transformation [*Buffett*, 2007; *Lay et al*., 2008] as well as lower mantle heterogeneity as imaged by seismic tomography interpreted in terms of temperature and compositional variations [*Monnereau and Yuen*, 2010; *Wu et al*., 2011]. These approaches generally indicate moderate amounts of lateral heterogeneity in CMB heat flux, with lateral variations of 20–30 mW m^{-2} [*Lay et al*., 2006, 2008; *Van der Hilst et al*., 2007].

However, the influence of this lateral thermal heterogeneity on CMB heat flux is amplified by lateral variations in thermal conductivity. High-pressure experiments [*Ohta et al*., 2012] and molecular dynamics calculations [*Ammann et al*., 2014] reveal that the thermal conductivity of ppv is higher than pv by nearly 50% at lower mantle conditions. Since ppv is concentrated in the lower-temperature regions above the CMB, where the thermal gradients are greatest, it boosts the CMB heat flux in these regions. Conversely, the poorly conducting pv is concentrated in the higher-temperature regions above the CMB, where the thermal gradients are probably lower than average. This has the effect of further reducing the CMB heat flux in these regions.

In terms of temporal variability, considerations of the evolution of the core based on its composition and the thermodynamics of the geodynamo generally indicate a monotonic increase in core heat flux going backward in time [*Driscoll and Bercovici*, 2014; *Nimmo*, 2015]. This smooth increase with age is partly due to

the predictable rate of increase in radioactive heat production and partly due to the fact that thermal evolution models usually assume only monotonic variations in the surface heat flow.

5. Heat Flux From Mantle GCMs

A somewhat different picture emerges from mantle GCMs. Mantle GCMs predict very strong lateral heterogeneity of the local CMB heat flux, and they also predict substantial variability in the global average CMB heat flux with time. The development of mantle GCMs and their application to the evolution of the mantle-core system is best exemplified in the sequence of papers by *Nakagawa and Tackley* [2005, 2008, 2010, 2012, 2013, 2015], in which ever more sophisticated representations of mantle rheology and thermodynamic properties have been added over time. Mantle GCMs that explicitly include surface plate motion constraints have been developed by *McNamara and Zhong* [2004] and *Bunge et al*. [2003], *Phillips and Bunge* [2005], and *Bull et al*. [2014] and greatly refined by S. Zhong and coworkers [*McNamara and Zhong*, 2005; *Zhang et al*., 2010; *Zhang and Zhong*, 2011; *Rudolph and Zhong*, 2014].

In order for Mantle GCMs to reconstruct the thermal history of the CMB region, they must incorporate the history of plate motions over several mantle overturns, in addition to the physical properties that control the circulation. Figure 5 illustrates schematically how these types of mantle GCMs are built. The important components are (1) a structural model for the mantle, specifying physical and thermodynamic properties, including the density profile, phase transitions, heat sources, and thermal boundary conditions; (2) viscosity laws for each region of the mantle, preferably with the viscosity being dependent on pressure (i.e., depth), temperature, and possibly composition and strain rate [*Nakagawa and Tackley*, 2011]; and (3) upper surface velocity boundary conditions derived from plate reconstructions. Plate reconstructions based on ocean floor data extend back in time only to 150–200 Ma [*Seton et al*., 2012], so that the surface velocity boundary condition becomes evermore poorly known with increasing age. Continent reconstructions have been used to derive low-resolution models for plate velocities and plate boundaries at ages older than 200 Ma [*Zhang et al*., 2010; *Torsvik and Cocks*, 2004; *Domeier and Torsvik*, 2014], but with large uncertainties.

Despite the uncertainties in rheology and thermodynamic properties, and despite of the shortcomings related to the time limits on plate motion reconstructions, mantle GCMs offer three major advantages over other methods for modeling and interpreting mantle history. First, they are based on the accepted equations of motion and therefore have a level of internal dynamical consistency that is lacking in more ad hoc, kinematic approaches. Second, they are reproducible, since the software and input data are widely shared within the mantle dynamics community (see Computational Infrastructure for Geodynamics, www.geodynamics.org, for example). Third, they can be improved incrementally, as new data on mantle structure, mantle properties, or new plate reconstructions become available. The broad applicability of mantle GCMs is evidenced in their use for predicting a wide variety of signals, including sea level change, variations in ocean crust production, polar motion, and the Wilson cycle of supercontinent aggregation and breakup [*Zhang et al*., 2010; *Bull et al*., 2014; *Bower et al*., 2013; *Li et al*., 2015; *Rudolph and Zhong*, 2014], to name just a few.

The CMB heat flux predicted by mantle GCMs depends on many inputs, including mantle viscosity, mantle heat sources, compositional heterogeneity, plate motion history, and thermal structure. As with other mantle GCM predictions, uncertainties in these properties lead to substantial uncertainty in the CMB heat flux. Nevertheless, a portion of this uncertainty can be removed by tuning the physical parameters so that the GCM matches the present-day mantle structure and surface observables, including the surface heat flux. It has been shown that formation and maintenance of dense chemical piles in the lower mantle constitute a powerful constraint on the global-scale properties of GCMs in the deep mantle [*McNamara and Zhong*, 2004, 2005], including the large-scale structure of heat flux on the CMB [*Zhang and Zhong*, 2011]. Specifically, it has been shown that very high CMB heat flux is required to support dense piles comparable to the Large Low Shear Velocity Provinces, the so-called LLSVPS, seen in seismic images of the present-day lower most mantle [*Dziewonski et al*., 2010; *French and Romanowicz*, 2015]. Maintaining dense piles comparable in size to the observed LLSVPs requires an average CMB heat flux of 75–100 mW m^{-2} with lateral variability of the same order, according to mantle GCM results [*Zhang et al*., 2010; *Zhang and Zhong*, 2011; *Olson et al*., 2013, 2015].

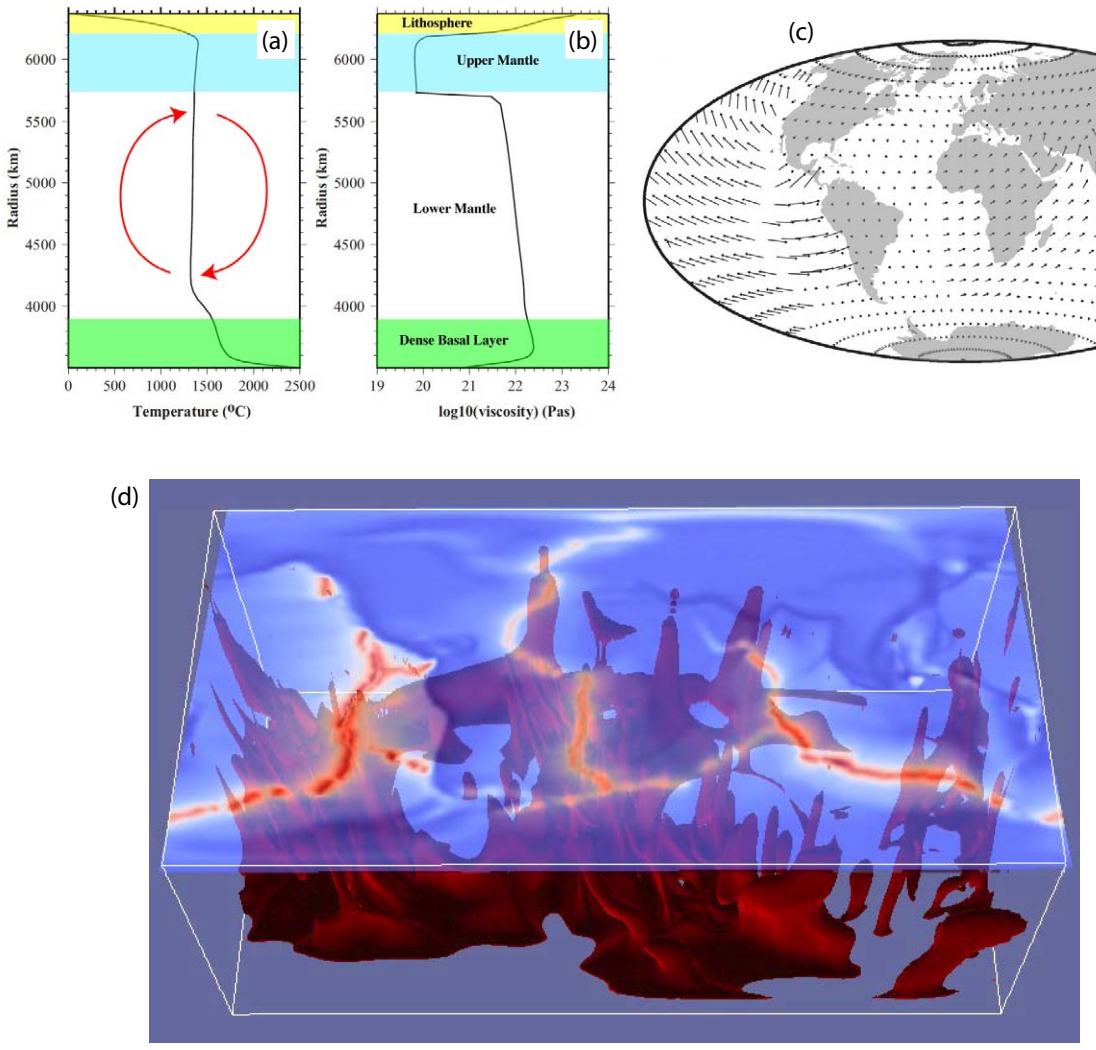

Figure 5. Ingredients of a mantle GCM. (a) Mantle density structure, thermal boundary conditions, and internal heat sources for free convection. Solid curve is a reference global average geotherm with the mantle adiabatic gradient removed. (b) Mantle viscosity structure (solid curve) with variations representing the lithosphere, upper mantle, lower mantle, and dense basal layer. (c) Plate velocity pattern used as a surface velocity boundary condition. (d) Snapshot of lower mantle thermal heterogeneity from a mantle GCM (isothermal surface in red) with overlay showing melt production at plate spreading centers.

As discussed earlier, mantle GCMs also predict nonmonotonic temporal variations in the global mean heat flux, both on the surface and on the CMB. On the CMB in particular, fluctuations in the global mean heat flux of ± 20 mW m^{-2} over Phanerozoic time are typical in these models [*Bunge et al*., 2003; *Nakagawa and Tackley*, 2010; *Zhang and Zhong*, 2011]. Figure 6 shows time series of the global average CMB heat flux versus time from mantle GCMs using a three different sets of plate motion reconstructions as surface boundary conditions [*Lithgow-Bertelloni and Richards*, 1998; *Müller et al*., 2008; *Seton et al*., 2012]. The plate motion reconstructions go back to 200 Ma or less; prior to that, the surface velocity boundary conditions come from syntheses by *Zhang et al*. [2010] of images from Paleomap [*Scotese*, 1997, 2001]. The global mean CMB heat flux in these three GCMs varies between 79 and 94 mW m^{-2}, with a time average around 86 mW m^{-2}, equivalent to 13 TW for the time average total core heat loss.

The dashed lines in Figure 6 indicate approximate values of the heat flux conducted down the core adiabat at the CMB, assuming different values of the Gruneisen parameter γ below the CMB. For $\gamma = 1.2$, all three mantle GCMs predict slightly superadiabatic conditions beneath the CMB over the whole time. For $\gamma = 1.35$, however, the GCM core heat flux is above adiabatic only around 70 Ma when plate speeds were highest, and subadiabatic at most times before and after. For $\gamma = 1.5$, the average thermal gradient beneath the

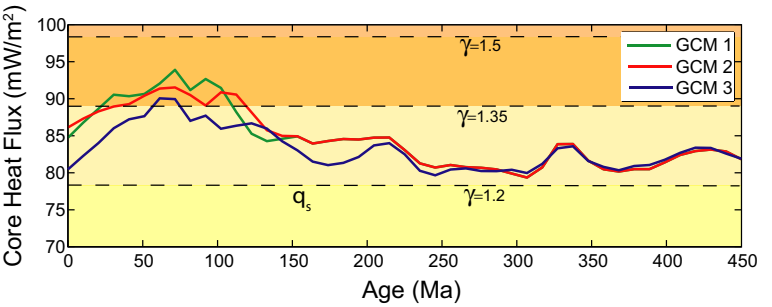

Figure 6. Global average CMB heat flux from three mantle GCMs, driven by the plate reconstructions described in the text. Reference adiabatic heat flux values q_s for different values of the Gruneisen parameter γ in the outer core below the CMB are indicated.

CMB would be subadiabatic during essentially all of time shown. In the following sections, we discuss the implications of this possibility for the geodynamo, both at present and in the past.

The peak in the averages CMB heat flux between 70 and 120 Ma in Figure 6 and the 10–20% decrease since that time mirror the time variations in surface heat flux inferred from seafloor ages. Temporal variations in oceanic spreading and crustal production rates have been calculated from plate age distributions going back nearly 180 Ma [*Cognè and Humler*, 2004; *Loyd et al*., 2007; *Becker et al*., 2009] and indicate comparable variations. *Becker et al*. [2009] showed that the so-called "triangular" distribution of crustal age versus preserved area in the present-day seafloor inventory is consistent with a 25–50% reduction of ocean floor spreading rates since 140 Ma. Converting this to heat flux, they predict a near 30% reduction in oceanic heat flux over this same time period, a reduction rate similar to that found by *Loyd et al*. [2007] for 0–60 Ma.

Time variations in CMB heat flux generally correlate with time variations in surface heat flux in most mantle GCMs because of the deep subduction teleconnection, although there may be a time lag between the two. When subduction rates are high, the mantle general circulation is energized and heat flux at the CMB rises. As described in the next section, the influence of a high subduction rate tends to be magnified at the CMB. Not only does the global mean heat flux increase, but also, the energized circulation sweeps the dense material at the base of the mantle into piles with smaller footprints, exposing more of the CMB to the direct effect of mantle downwellings and thereby increasing the lateral heterogeneity of the CMB heat flux. In addition, postperovskite, which forms at the base of the mantle downwellings, covers a greater portion of the CMB, and its higher thermal conductivity compared to perovskite further increases the mean CMB heat flux and its lateral variability. This is a prime example of top-down regulation of the mantle-core system in action.

It should be noted that, although the surface and the CMB heat flux tend to be correlated overall, some mantle GCMs predict a time lag in their interaction. The nominal situation is that CMB variations lag surface variations, in some models by a few million years [*Zhang and Zhong*, 2011] and in others by a few tens of millions of years [*Bunge et al*., 2003; *Nakagawa and Tackley*, 2010], the difference being due to the amount of mechanical resistance experienced by subducted material as it sinks from the upper mantle into the lower mantle in the various models. Significantly, none of these models show the CMB heat flux variations leading the surface heat flux variations in time, as expected in the "bottom-up tectonics" scenarios, wherein the dynamics of the lower mantle are assumed to control mantle dynamics nearer the surface [*Romanowicz and Gung*, 2002; *Dziewonski et al*., 2010].

In part, the bottom-controlled scenario is not evident in mantle GCMs because the circulation in most GCMs is dominated by the surface plate motion. The surface domination of the lower mantle in these models might be exaggerated compared to what actually occurs, however. Evidence for this comes from LIP reconstructions, which show that the dominant spherical harmonic degree 2 lower mantle heterogeneity of the present day is more persistent through Earth history than most GCMs predict [*Torsvik et al*., 2008]. Additional evidence for lower mantle activity not directly tied to plate motions comes from the heightened LIP activity during the mid-Cretaceous plume pulse [*Larson*, 1991], an event which mantle GCMs fail to reproduce. In short, although their overall top-down control is probably correct to first order, there is ample room for improving GCM dynamics in the deep mantle.

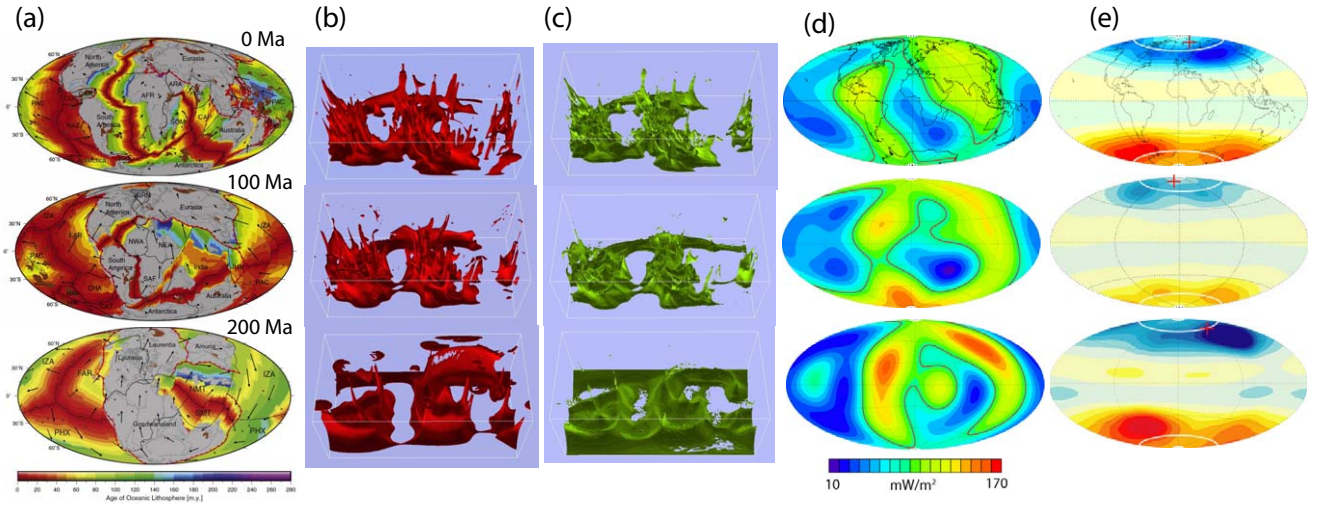

Figure 7. Top-down regulation of the core and geodynamo by the global mantle circulation. Rows (from bottom to top) show evolution of a coupled mantle-core system model at three ages. Columns from left to right: (a) Continent configuration, ocean crust ages, and plate motions from *Seton et al*. [2012] reconstruction; (b and c) lower mantle thermal (red) and compositional (green) heterogeneity from mantle GCM; (d) CMB heat flow from mantle GCM, truncated at spherical harmonic degree and order 4, with solid line delineating thermally stable and unstable sub-CMB regions; and (e) time-averaged radial magnetic field intensity on the CMB from the numerical dynamo. Red and blue correspond to outward and inward radial magnetic field; red cross marks the axis of the geomagnetic dipole.

6. Top-Down Regulation in an Earth System Model

Figure 7 illustrates the workflow in an Earth System Model with top-down regulation, consisting of a mantle GCM with surface plate motion constraints thermally coupled to a numerical dynamo for the core using the boundary conditions derived previously.

Moving from left to right in Figure 7, the first column shows surface plate velocity patterns, ocean crust ages, and continent positions at 0 (present day), 100, and 200 Ma, from a plate reconstruction by *Seton et al*. [2012]. The second and third columns show the lower mantle heterogeneity at these times in terms of temperature and composition, respectively, from a mantle GCM by *Zhong and Rudolph* [2015] that is driven by the *Seton et al*. [2012] plate reconstruction. The fourth column shows the heat flux on the CMB from the mantle GCM, truncated at spherical harmonic degree $\ell = 4$ in order to filter out the unreliable shorter wavelength heterogeneity. The fifth column shows the time-averaged radial component of the magnetic field on the CMB produced by the numerical dynamo driven by the CMB heat flux patterns in the fourth column.

In terms of plate motions, the primary tectonic action in the lithosphere since 200 Ma involves the breakup of Pangaea, the formation of oceanic spreading centers surrounding the African continent, and their propagation throughout the Atlantic and Indian Ocean basins. However, the main effects on the core stem from the pattern of subduction and its changes with time. As former lithospheric material from subduction off the western margins of North and South America and the persistent subduction complexes surrounding East Asia sinks through the lower mantle, two large holes are excavated in the compositionally dense material lying above the CMB. The local heat flux on the CMB is very high at these excavations, exceeding 130 mW m^{-2} in places. The dense material mobilized by the spherical harmonic degree 2 dominant pattern of mantle downwellings accumulates in two major piles, one centered beneath southern Africa, the other with its center beneath the central Pacific, just south of the equator. At these locations, the heat flux on the CMB is quite low, falling below 30 mW m^{-2} in places. Both the existence and the persistence of the compositional piles contribute to the extreme heterogeneity of heat flux on the CMB; its peak-to-peak variation in this mantle GCM (nearly 100 mW m^{-2}) exceeds the global mean heat flux (80–95 mW m^{-2}), even when the smoothing effect of the $\ell = 4$ truncation is applied.

The solid contours on the CMB heat flux maps in Figure 7d separate regions in the outer core beneath the CMB that are expected to be superadiabatic (thermally unstable) and subadiabatic (thermally stable), assuming an adiabatic heat flux of 86 mW m^{-2}. At 100 Ma, approximately 50% of the CMB area lies in each state, whereas only about 40% would be superadiabatic at present, according to this mantle GCM. The regions where the outer core is thermally unstable beneath the CMB lie underneath holes in the dense

compositional layer produced by downwellings that are analogs of the trajectories of deep subduction in the mantle. For an adiabatic heat flux of 100 mW m^{-2}, there would still be substantial thermally unstable areas beneath these mantle downwellings. Conversely, the regions where the outer core is thermally stable (i.e., subadiabatic) lie underneath the compositional piles, analogs of the seismic LLSVPs in the lower mantle. For an adiabatic heat flux of 100 mW m^{-2}, these regions would cover most (but not all) of the CMB.

The effects of the CMB heat flux heterogeneity on the long-term structure of the core dynamo are shown in the last column, in terms of the time-averaged intensity of the radial component of the magnetic field on the CMB. These magnetic field structures were calculated using the dynamo model and the methods described in *Olson et al*. [2013], subject to the CMB heat flux patterns shown in Figure 7d, and assuming the solid contour divides thermally stable and unstable regions in the outer core. Deviations from purely axial symmetry are evident in the magnetic field structure at all ages. At 0 and 100 Ma, the expression of the dominant spherical harmonic degree and order 2 structure of the mantle heterogeneity is seen in the nonaxial field, in the form of lobes of high-magnetic intensity positioned slightly west of the longitudes of maximum CMB heat flux, in both the northern and southern hemispheres. In spite of this nonaxial structure, however, the dipole component of the magnetic field is dominantly axial at these times, as shown by the proximity of the dipole axes (marked by red crosses) to the rotation axis at these times.

The situation is different at earlier times in Figure 7, at 200 Ma in particular, which is just as the breakup of Pangaea got underway. Prior to and during that time, mantle GCMs with plate motion constraints predict the existence of a large spherical harmonic degree and order 1 signal in the mantle structure, including the CMB heat flux [*Zhang and Zhong*, 2011; *Olson et al*., 2013]. This degree 1 mantle structure is reflected in the dynamo magnetic field in the form of a single major high-intensity lobe in each of the northern and southern hemispheres. Because the northern flux lobe lies in the eastern hemisphere and the southern flux lobe lies in the western hemisphere, the magnetic dipole axis is tilted, inclined to the rotation axis by approximately 20° at this time.

Persistent tilt of the geomagnetic dipole axis is a controversial issue. Traditionally, most paleomagnetic studies explain global-scale, systematic magnetic inclination anomalies in terms of true polar wander, i.e., rotation of the mantle relative to Earth's spin axis [*Besse and Courtillot*, 2002], rather than long-lived geomagnetic dipole axis tilt. Nevertheless, as Figure 7 shows, the geodynamics of the core-mantle system raises the possibility—even the likelihood—that the time-averaged dipole has been tilted (and also offset) from the spin axis during some periods of Earth history. This applies particularly at times of supercontinent formation, when the dominant spherical harmonic degree 2 structure of the mantle may weaken.

The movement of the dipole axis implied by its positions at 200 and 100 Ma in Figure 7e would be seen as equivalent to an apparent rotation of the continents by approximately 25° in the clockwise sense about an equatorial axis located near 0° East Longitude. For example, North America and Eurasia would appear to rotate toward and away from the spin axis with time, respectively, due to this effect. Significantly perhaps, these apparent rotations are comparable in both magnitude and direction to what has been inferred by *Steinberger and Torsvik* [2008] for the period 195–145 Ma on the basis of paleomagnetic directions, motions they interpret as uniform rotation of the lithosphere, i.e., classic true polar wander.

Could geomagnetic dipole wander (rotation of the dipole axis) contribute to apparent polar wander, and could it be confused with true polar wander (rotation of the lithosphere)? Likewise, how reproducible are the dipole offsets in the numerical dynamos shown here? In general, the departure from the geocentric axial dipole configuration depends on the magnitude and the asymmetry of the CMB heterogeneity, which tend to promote dipole tilt, versus rotational control, which tends to suppress it. The dynamo calculations in Figure 7 have rather weak rotational control. In addition, the plate reconstruction that produces the patterns of CMB heterogeneity shown in Figure 7 assumes a geocentric axial dipole field a priori. Accordingly, there are grounds for questioning the reliability of these pole positions. A more rigorous test would be to start with a lower Ekman number (faster rotating) dynamo, apply arbitrary rotations to the CMB heterogeneity pattern from the GCM, and search for self-consistency between the dynamo-calculated dipole axis location and the dipole axis location implied by the continent positions using the geocentric axial dipole assumption. To this authors knowledge, no such test has ever been done with a numerical dynamo. However, because the geocentric axial dipole assumption lies at the heart of many paleo-reconstructions, internally consistent calculations of this type merit some consideration.

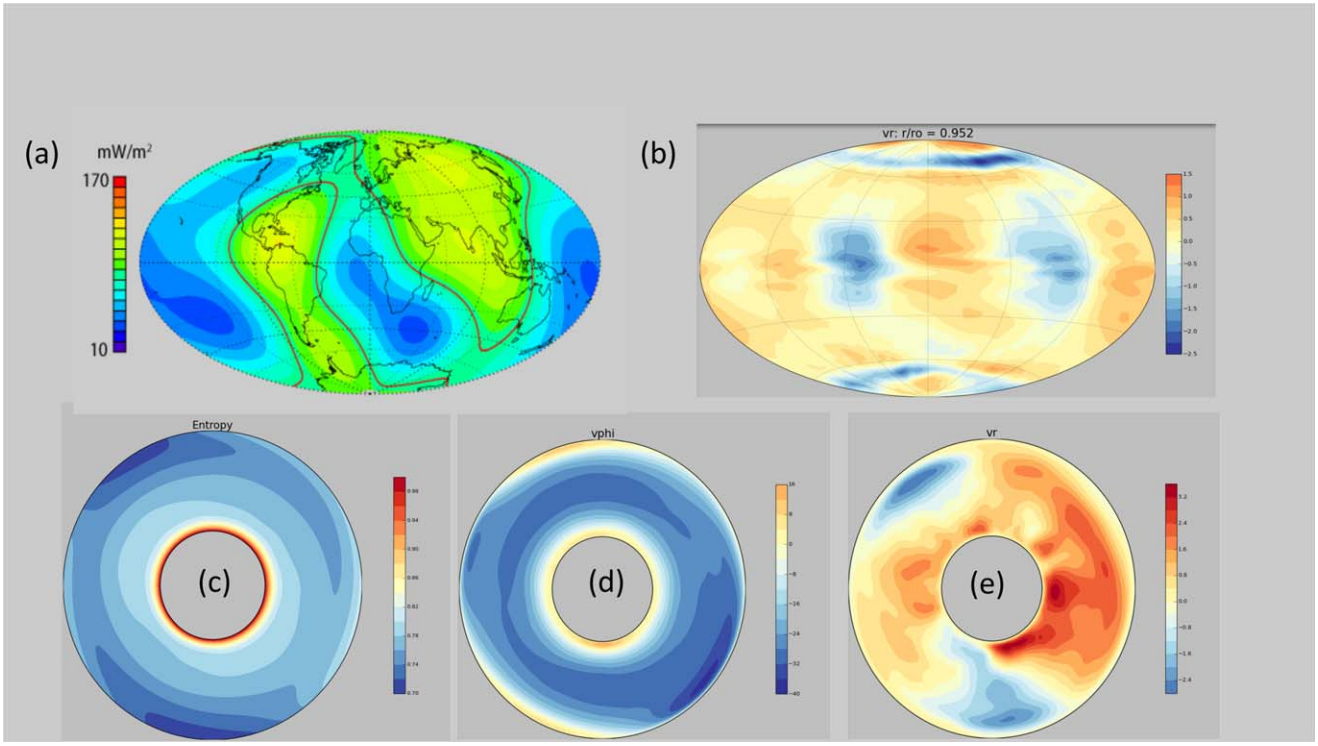

Figure 8. Time-averaged structure of the core subject to CMB heat flux heterogeneity, from the numerical dynamo with high thermal conductivity, as described in the text. (a) Present-day CMB heat flux from a mantle GCM; (b) radial velocity at $0.95r_{cmb}$; (c) codensity (entropy) in the equatorial plane; (d) azimuthal velocity in the equatorial plane; (e) radial velocity in the equatorial plane. Longitude 0° is to the left in these images; all dynamo quantities are in nondimensional units.

Figure 8 shows more detail on how mantle dynamics controls the geodynamo. Figure 8a shows the present-day CMB heat flux pattern from a mantle GCM [*Zhong and Rudolph*, 2015] applied as the outer thermal boundary condition on a numerical dynamo in which the driving force for convection in the outer core is a combination of thermal buoyancy provided by the heat flux at the CMB and compositional buoyancy provided by a flux of light elements at the inner core boundary, the product of core cooling. The combination of these two buoyancy sources is represented in the dynamo model in terms of the codensity variable,

$$C=\rho_{oc}(\alpha T+\beta\chi), \tag{5}$$

where ρ_{oc} denotes outer core density, T the outer core temperature relative to the adiabat, χ the outer core light element composition (the light elements being an unknown mixture of oxygen, sulfur, silicon, and possibly other elements lighter than iron) [see *Hirose et al*., 2013], and α and β are volumetric expansion coefficients for T and χ, respectively. In terms of dimensionless parameters, the dynamo in Figure 8 has a Rayleigh number $Ra=8\times10^6$, Ekman number $E=10^{-4}$, Prandtl number $Pr=1$, magnetic Prandtl number $Pm=6$, the dimensionless mean CMB codensity flux is 0.2, the peak-to-peak variation boundary variation is approximately 0.4, and the stable region occupies, on average, about 20% of the outer core beneath the CMB. Other dynamo model details are given in *Olson et al*. [2015].

The spherical mean CMB heat flux in this dynamo is subadiabatic, but the extreme lateral heterogeneity of the boundary heat flux generates a combination of superadiabatic and subadiabatic regions beneath the CMB. As Figure 8 shows, the patchwork of thermally stable and unstable regions below the CMB affects the entire core. First, it generates a circulation pattern in the outermost portion of the outer core that is strongly tied to the pattern of the CMB heat flux, particularly at low latitude and midlatitude. There, locally concentrated downwellings and upwellings occur beneath the regions with high and low CMB heat flux, respectively, as shown in Figure 8b. The extent of the boundary-tied downwellings depends somewhat on the structure of the outer core beneath them, but for the most part they are limited to the top few hundred kilometers of the outer core, as Figure 8e reveals. In contrast, the upwelling regions are more extensive and

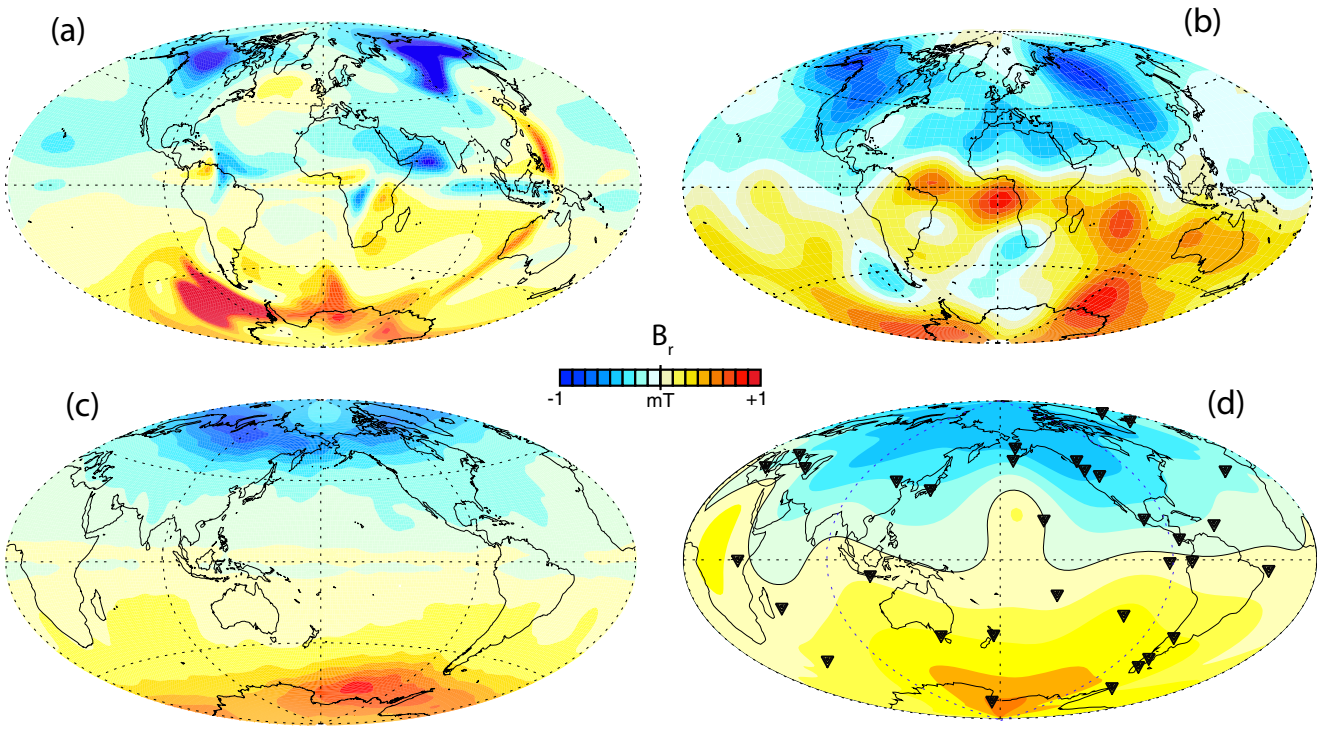

Figure 9. Comparison of numerical dynamo with high core conductivity and heterogeneous CMB heat flux with present-day and time-averaged geomagnetic field. Shown are contours of the radial magnetic field intensity on the CMB, in mT (millitesla) for the geomagnetic field and in dimensionless units for the numerical dynamo. (a) Numerical dynamo snapshot; (b) present-day core field (Pomme 6 model); (c) time-averaged numerical dynamo field; (d) 0–5 Ma time-averaged geomagnetic field from *McFadden and Johnson* [2015].

stronger, extending upward from the ICB, especially in the Pacific hemisphere. The net outward mass flux implied by these upwellings is balanced by a poleward meridional circulation, with enhanced downwellings located near the tangent cylinder of the inner core as shown in Figure 8b. In spite of their greater strength, the upwellings originating at the ICB experience strong attenuation on approach to the CMB from below, as they encounter the stable stratification.

The downwellings tied to CMB heat flux maxima are strong enough to locally reverse the direction of the azimuthal component of the general circulation below the CMB. Figure 8d shows that the generally retrograde (i.e., westward) azimuthal flow reverses and becomes prograde (i.e., eastward) just downstream (westward) of the CMB heat flow maxima, forced by the strong, localized downwellings. Elsewhere, the dominant westward azimuthal flow is strengthened, especially near the longitudes where the CMB heat flux is minimum. Combining the information in Figures 8b, 8d, and 8e reveals that the lateral variability of the CMB heat generates localized circulations below the CMB that bear some dynamical resemblance to the tropospheric Walker cells associated with the El Nino and La Nina states of the subtropical atmosphere.

We can identify signatures of these localized outer core circulations in the external geomagnetic field by comparing the structure of the main part of the present-day geomagnetic field with snapshots of the magnetic field from numerical dynamos with CMB heterogeneity. Figures 9a and 9b show such a comparison, in this case, between a snapshot from the numerical dynamo described in Figure 8 and the radial component of the present-day geomagnetic field on the CMB from the Pomme 6 2010 core field model (https://geomag.colorado.edu/geomagnetic-and-electric-field-models.html).

The pattern of intensity of the radial field in the dynamo model snapshot in Figure 9 shows qualitative resemblance to the present-day geomagnetic intensity, and several points of resemblance can be attributed to the lateral variations in CMB heat flux. First, the numerical dynamo snapshot has high field intensity patches beneath North America and Eurasia at approximately the same longitudes and latitudes as in the present-day geomagnetic field. In the southern hemisphere, the high field intensity structure is less symmetric in both the model and the Earth. Nevertheless, there is a general correspondence in terms of the latitude and longitude of the patches. Another qualitative resemblance is the band of high-intensity field

extending north-to-south beneath the Indian Ocean, from the coast of Antarctica to near the equator, present as a narrow structure in the dynamo model and a much broader and more intense structure in the core field. This structure bends to the west just south of the equator, where it connects with other spots of high-intensity field beneath subequatorial Africa and, in the case of the present-day core field, extends beneath the equatorial Atlantic. It partially encloses spots where the field has reversed polarity, with weakly reversed field in the model snapshot and stronger reversed field in the present-day core. In the present-day core field, these reversed polarity spots are collectively the source of the geomagnetic South Atlantic Anomaly (SAA), because they combine to produce a large region of low-intensity field with enhanced levels of charged particle fluxes at satellite altitudes [*Abdu et al*., 2005]. There is paleomagnetic evidence that the SAA is an ancient feature, tied to mantle heterogeneity [*Tarduno et al*., 2015b], a regional-scale manifestation of top-down control of the geodynamo by the mantle.

Second, the strengths of nondipole field structures beneath the Pacific are substantially less than their counterparts beneath the Atlantic and Africa, in both dynamo model and geomagnetic fields. This is a persistent imbalance in the dynamo model, having to do with the fact that the high CMB heat flux longitudes are closer together beneath the Atlantic in Figure 8a, compared to their spacing beneath the Pacific. Low-intensity and generally weak geomagnetic secular variation in the present-day core field has long been noted [*Bloxham et al*., 1989], although on longer time scales, it appears wax and wane [*Coe et al*., 1978]. A proposed dynamo-generated source of the Atlantic-Pacific discordance is the east-west dichotomy in the growth rate of the inner core [*Aubert et al*., 2013]; this mechanism may itself be a product of CMB heterogeneity [*Aubert et al*., 2008].

Third, there are local minima in the field intensity at or very near the poles, in both dynamo model and present-day field geomagnetic structures, especially in the present-day north polar region of the geomagnetic field, where many core field models (including Pomme 6 in Figure 9) actually have reversed polarity field in this region. In numerical dynamos, these polar minima are due to convective upwellings that rise from the ICB toward the CMB along the rotation axis (shown in Figure 8b). As these upwellings diverge equatorward beneath the CMB, they transport magnetic field away from the poles, thereby weakening (and locally reversing) the field, creating polar minima [*Christensen et al*., 1998]. The geostrophic response to this equatorward flow is an even stronger prograde azimuthal flow, the so-called outer core polar vortex, for which there is evidence for in the historical geomagnetic secular variation [*Olson and Aurnou*, 1999].

The main effects of mantle heterogeneity survive in the long-term averages of the core field. Figures 9c and 9d compare the time-averaged numerical dynamo field with the 0–5 Ma time-averaged geomagnetic field from *McFadden and Johnson* [2015], both on the CMB. The high-intensity flux beneath North America and Eurasia remains both, although in each case, these structures are more attenuated than in the snapshots, forming lobes rather than distinct patches. In the southern hemisphere, the high-intensity patches merge into a single lobe, in both the geomagnetic field and in the numerical dynamo, reflecting the differences in CMB heat flux between the two hemispheres at high latitudes.

Finally, it is important to note that both the numerical dynamo and the geomagnetic field are extremely time variable, so that some of the similarities described here are not evident in every snapshot. In addition, the numerical dynamo field intensity is given in Figure 9 in nondimensional units and unfiltered by the crust, and therefore needs to be scaled to Earth's core conditions when comparing the absolute field intensity. But even with these caveats, there is clear manifestation of the mantle on the geomagnetic field.

7. Age of the Inner Core

In their pioneering development of mantle GCMs, *Nakagawa and Tackley* [2005, 2010] noted that models of mantle convection that best matched surface heat flux and lithospheric age distributions also predicted very high CMB heat flux. When coupled to an evolution model of the core, these GCMs predicted young inner core ages. At that time, there was widespread opposition to the concepts that the core-to-mantle heat flow could be so large and that the inner core might be so juvenile. Some of this opposition was based on core heat flow estimates derived from the observed buoyancy flux at volcanic hot spots [*Stacey and Loper*, 1983; *Labrosse*, 2002], thought to represent the heat transported from the deep mantle. However, the smallest of those estimates came from summing the upward buoyancy flux at volcanic hot spots, and these

mistakenly underestimated the equally important, upward buoyancy flux produced by cold mantle downwellings, which turns out to be a large contributor to the flux carried by plumes [*Zhong*, 2006].

Since then, the twin developments described in section 2—evidence for elevated CMB heat flux from seismology and geodynamics along with the new determinations of high thermal conductivity in the core—have forced a reexamination of the rate at which the core evolves. It is now widely accepted that the core is evolving (e.g., cooling) rapidly, and consequently, the inner core is relatively young. So, how young? In this section, I review the line of reasoning that the inner core is shockingly young, with a plausible upper bound of a bit more that 1 Ga, and equally significant, suggestions that it could be as young as 0.4 Ga. I also conjecture on what it implies for the history of the core and the longevity of the geodynamo that the inner core—thought to be its major power source—has only been around since Neoproterozoic or possibly even Phanerozoic times.

The main assumptions used in calculating the growth rate and the age of the inner core have survived decades of scrutiny, with little alteration. These are: (1) the ICB is at the melting point of the outer core liquid; (2) the outer core mixes heat and composition on time scales far shorter than its evolutionary time scale, so the core is always in approximate thermal equilibrium with the CMB, and in thermal and compositional equilibrium with the inner core at the ICB, and (3) apart from latent heat, the only significant internal heating is radioactive. Although estimates of the amount of radioactive heat in the core vary considerably [*Nimmo*, 2015], even the highest of these estimates barely changes the main story.

Subject to these assumptions, the rate of inner core growth, as it responds to the cooling of the core, can be written

$$\dot{r}_{ICB} = \frac{(Q_{cmb} - Q_{rad})}{P}, \tag{6}$$

where r_{ICB} is the inner core radius, Q_{cmb} and Q_{rad} denote the total core heat loss at the CMB and radioactive heat production, respectively, and $P = P_l + P_g + P_s$ is the summation of contributions to the core energy balance from latent heat release at the ICB, gravitational energy release, and secular cooling of the core, respectively. The individual contributions to P can be expressed in terms of core thermodynamic and structural properties [*Labrosse*, 2003]. Accordingly, the age of the inner core is directly proportional to P and inversely proportional to $Q_{cmb} - Q_{rad}$. Overall, P is most sensitive to the difference between the gradients of the core adiabat T_s and the melting curve T_{melt} at the ICB, i.e., the parameter $\Theta = \left(\frac{dT_s}{dr} - \frac{dT_{melt}}{dr}\right)\Big|_{\mathrm{icb}}$.

Mantle GCMs yield internally consistent estimates for the time variations in heat loss from the core, the critical input for calculating the evolution of the core, and predicting the age of the inner core using the formalism described above. However, mantle GCMs with plate motion constraints normally begin after ICN, so some extrapolation backward in time is necessary. Examples are shown in Figure 6. The small differences prior to 220 Ma are attributed to differences in the tracer methods that are used for tracking the compositional heterogeneity in the GCM. For these three plate reconstructions, the time and cross-model averages of the 0–200 Ma total core heat flow is $Q_{cmb} = 13 \pm 1.3$ TW. *Zhang and Zhong* [2011] investigated the sensitivity of CMB heat flux in mantle GCMs with and without the D″ chemically dense layer, for a variety of mantle viscosity structures and Clapyeron slopes of the transition zone phase transformations. Uncertainties in these parameters yield CMB heat fluxes in the range 80–110 mW m^{-2}, approximately 12–17 TW total. This range of core heat loss is comparable to other mantle GCMs that include chemical piles in the deep mantle [*Nakagawa and Tackley*, 2005, 2013].

Figure 10 shows contours of theoretical ICN ages versus Q_{cmb} and Θ, using the thermal evolution model of *Labrosse* [2003] with the core properties in *Olson et al.* [2015]. In terms of extremes ICN ages, Figure 10 range from just over 1600 Ma for $Q_{cmb} = 6$ TW to less than 400 Ma for $Q_{cmb} = 18$ TW. Considering just the mantle GCM-derived values of Q_{cmb}, this range reduces to 400–950 Ma, if no radioactive heating is present, which is the case shown here. The predicted age of ICN increases when core radioactive heat production is included, but the change is rather small for the plausible amounts of radioactive heating in the core. A plausible upper limit on present-day heat production in the core is about 1 TW [*Hirose et al.*, 2013; *Watanabe et al.*, 2014], but even with this amount, the maximum ICN age within the dashed box in Figure 10 only increases to about 1100 Ma.

An independent constraint on core evolution is its capacity for sustaining the geodynamo by convection, which turns out to add a powerful restriction on inner core age. The geomagnetic field has persisted since

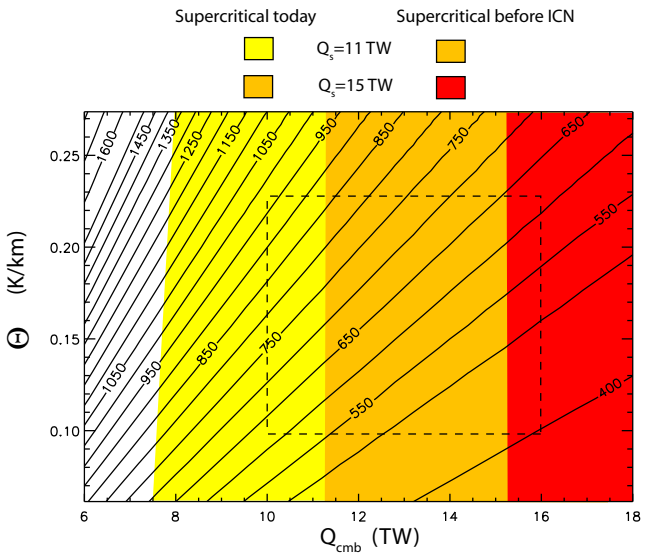

Figure 10. Age of the inner core predicted by thermal evolution models. Shown are contours of the age of inner core nucleation ICN in Ma as a function of total core heat flow Q_{cmb} and Θ, the difference between the melting point and adiabatic gradients at the present-day ICB. Color scheme shows dynamo states for two choices of the adiabatic heat flow at the CMB. Dashed square delineates predictions from mantle GCMs.

3400 Ma [*Tarduno et al*., 2010] and possibly since 4200 Ma [*Tarduno et al*., 2015a], so the core must support dynamo action before ICN as well as since. In Figure 10, the unshaded region denotes parameter combinations for which the core is subcritical for convection-driven dynamo action today, and the shadings indicate supercritical conditions for convective dynamo action today and just prior to ICN, for two different assumed values of the adiabatic core heat flow. These regions are defined in terms of a critical magnetic Reynolds number of 100 and are based on scaling laws derived by *Christensen and Aubert* [2006]. The two adiabatic heat flow choices shown in Figure 10 roughly correspond to the range of uncertainties in the thermal conductivity. The lower adiabatic heat flow is representative of the volume-averaged core conductivity predicted by *Zhang et al*. [2015] on the basis of an expanded density functional theory (DFT) that includes electron-electron scattering; the higher value comes from more traditional DFT calculations without this effect [*Pozzo et al*., 2014].

According to Figure 10, a CMB heat flow of 8–11 TW includes the minimum to maintain the geodynamo by convection in the present-day core. Before inner core nucleation, however, the requirements were more stringent. The darker shadings in Figure 10 correspond to parameter combinations for which the core is supercritical for convective dynamo action just prior to ICN. This region includes only large Q_{cmb}-values and generally young inner core ages, particularly with the adiabatic heat flow associated with high thermal conductivity. The maximum inner core age for which the geodynamo was supercritical prior to ICN is approximately 850 Ma for Q_s= 11 TW, according to these calculations. For Q_s= 15 TW, the maximum IC age is only about 650 Ma, and more than 15 TW of core heat flow would be needed prior to ICN. For reference, with 13 TW of heat loss, the present-day cooling rate of the core is around -0.13 K Myr^{-1} at the CMB, and since the ICN, the CMB temperature has decreased by less than 100 K since that time.

The time of ICN clearly represents an important calibration point in the evolution of the Earth, and according to the above calculations, mantle control of the core favors a very young inner core. These ICN estimates are purely theoretical, however, and as yet there is no independent, conclusive evidence as to the timing of ICN. One obvious place to search for evidence of the ICN is the paleomagnetic record, where a shift in paleomagnetic field intensity [*Aubert et al*., 2009], a permanent change in magnetic field morphology, or a permanent change polarity reversal behavior might signal the onset of the additional driving forces due to inner core solidification. Unfortunately, no such permanent shifts in any of these paleomagnetic indicators have been found. For example, roughly stationary polarity reversal behavior has been found back to nearly 2.3 Ga, including evidence for magnetic superchrons over this entire time interval [*Driscoll and Evans*, 2016]. In addition, there is no evidence for a permanent shift in paleomagnetic field intensity [*Tauxe and Yamazaki*, 2007; *Biggin et al*., 2015].

There is, however, evidence in Proterozoic paleointensity records for periods of time when the geomagnetic field was weak, which could plausibly locate the ICN. Figure 11 shows virtual axial dipole moment (VADM) and virtual dipole moment (VDM) determinations between 0.5 and 2.8 Ga compiled from the PINT database by *Biggin et al*. [2015]. The range of ICN ages predicted by mantle GCMs is indicated, along with an ICN age near 1.5 Ga proposed by *Biggin et al*. [2015] that coincides with an apparent dipole moment minimum followed by a strong maximum that might signal the ICN. Although there are several implied minima and maxima, the data lack a clear trend or obvious shift, and there is much scatter. Indeed, Figure 11 shows that the time average

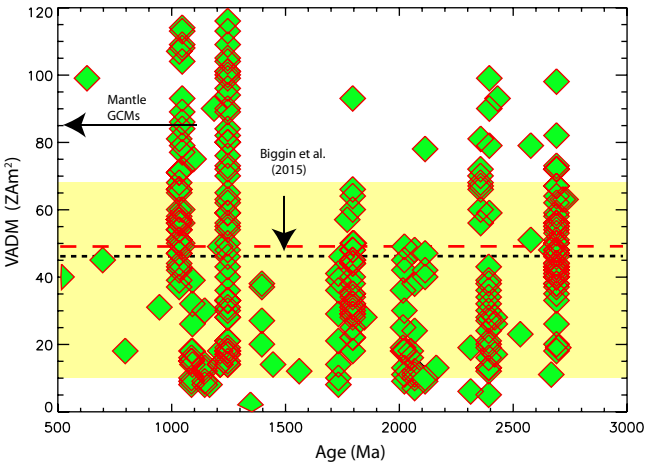

Figure 11. Proterozoic paleomagnetic intensity. Diamonds: virtual axial dipole moment (VADM) and virtual dipole moment (VDM) determinations between 0.5 and 2.8 Ga from *Biggin et al.* [2015], in units of ZAm^2 ($=10^{21}$ Am^2). Red dashed line: time average of Proterozoic VADM; yellow shading: Proterozoic dipole moment standard deviation; black dashed line: Phanerozoic dipole moment time average from *Selkin and Tauxe* [2000]; proposed ICN ages based on paleointensities: vertical arrow = *Biggin et al.* [2015] and horizontal line = mantle GCMs.

paleointensity in the Phanerozoic (most likely, post-ICN) is essentially indistinguishable from the intensity in the Proterozoic (most likely, pre-ICN). In addition, dynamo scaling laws are somewhat ambiguous in their predictions of field intensity with the inner core versus without the inner core [*Aubert et al.*, 2009], so it is not obvious that paleomagnetic intensity should spike following ICN. In short, although the ICN represents a benchmark event in deep Earth history, pinning down its timing remains a challenge.

8. Old Problems, New Approaches

Most of the topics discussed in this review involve long-standing problems that have proven their immunity to easy solution. Nevertheless, some new and potentially fruitful avenues of approach have been identified. For example, the greatest impediment to unraveling the long-term history of core-mantle interaction is the limited time during which surface plate motions are known. Comprehensive, global reconstructions of plate velocities go back to about 200 Ma [e.g., *Seton et al.*, 2012] and more limited reconstructions based on continent reconstructions, such as provided by *Scotese* [2001] or *Domeier and Torsvik* [2014] have been built that allow GCMs to go 200×10^6 years further back in time [*Zhang et al.*, 2010]. However, these older reconstructions have substantially larger errors, and most importantly for mantle circulation, they poorly constrain oceanic plate boundaries.

In addition to the time limits of the plate reconstructions, Mantle GCMs make assumptions about the temperature and pressure dependence of viscosity and the extent of compositional heterogeneity, issues that are still under debate. Uncertainties resulting from our incomplete knowledge of these properties will likely persist for a long time. Mantle GCMs also need more time variability, if they are to account for "black swans," less predictable events in the mantle history such the mid-Cretaceous plume pulse, a major perturbation originating in the lower mantle that may have provoked a geomagnetic superchron [*Larson and Olson*, 1991; *Biggin et al.*, 2012]. More immediately on the horizon, mantle GCMs have the capacity to assimilate new types of geophysical and geochemical data, thereby offering ways to overcome some of the limitations listed above. For example, there has been significant progress in implementing melt production and melt composition in mantle GCMs [*Li et al.*, 2015]. This brings in the capability to assimilate petrologic data, crustal thickness data, as well as crustal age data at ocean plateaux and from continental flood basalt provinces. Last, there have been significant theoretical progress toward a first-principles theory of plate boundaries, in particular, the damage theory developed by *Bercovici and Ricard* [2014]. Incorporation of lithospheric damage concepts or other first-principles approaches in mantle GCMS would allow more self-consistent dynamical interactions between plates and the mantle.

On the core side of the CMB, there is increased need to resolve outer core stratification—determine its radial extent, quantify its stability in terms of buoyancy frequency, and delineate the proportions that thermal and compositional effects contribute to it. In that regard, a key milestone would be on a definitive model for the light element composition of the core, which is, unfortunately, a multidecade objective that is still unsettled [*Hirose et al.*, 2013]. In terms of modeling, the need for improved numerical dynamos is well documented [*Matsui et al.*, 2016]; less well documented but equally important in the context of core-mantle interactions are numerical dynamos with realistic boundary conditions and an internal density structure that faithfully represents the observed departures from homogeneity in the outer core. These

improvements are needed to better address questions such as mantle-driven departures from axial dipole configurations in the time-averaged paleomagnetic field.

As for the evolution of the core and the geodynamo, the final words on the transport properties in the core and lower mantle are probably not in yet. If recent history is a guide, there will be revisions to our current estimates of these properties, particularly the thermal conductivity of core compounds and the postperovskite phase in the lowermost mantle, which could profoundly alter our current interpretations of core-mantle interaction. Alternative dynamo power sources remain a distinct possibility, especially for the ancient geomagnetic field. In this regard, the list of usual suspects (tides, precession, etc.) has been augmented by precipitation of low-solubility light elements from the outer core [*O'Rourke and Stevenson*, 2016]. Finally, a major breakthrough would be the detection of the ICN in paleomagnetic or other geophysical data. The timing of the onset of inner core solidification is an important benchmark in the evolution of the core, and as well as for the long-term evolution of the mantle. ICN times have been proposed recently on the basis of weak paleomagnetic intensity, but the definitive signature of this event remains unclear.

Acknowledgments

Support from Frontiers in Earth System Dynamics grant EAR-1135382 from the National Science Foundation is gratefully acknowledged, along with very helpful reviews by Ulrich Christensen, one anonymous referee, and Andy Biggin, who kindly pointed to the paleointensity data presented in this paper, available at http://earth.liv.ac.uk/pint/. Mingming Li created the 3D mantle GCM images. Conflicts of interest: author has no conflicts of interest to disclose regarding this research or this paper. Author contributions: P.O. made the interpretations, did the analysis, and the writing.

References

Abdu, M. A., I. S. Batista, A. J. Carrasco, and C. G. M. Brum (2005), South Atlantic magnetic anomaly ionization: A review and a new focus on electrodynamic effects in the equatorial ionosphere, *J. Atmos. Sol. Terr. Phys.*, *67*(17), 1643–1657.

Amit, H. (2014), Can downwelling at the top of the Earth's core be detected in the geomagnetic secular variation?, *Phys. Earth Planet. Inter.*, *229*, 110–121.

Ammann, M. W., A. M. Walker, S. Stackhouse, J. Wookey, A. M. Forte, J. P. Brodholt, and D. P. Dobson (2014), Variation of thermal conductivity and heat flux at the Earth's core-mantle boundary, Earth *Planet. Sci. Lett.*, *390*, 175–185.

Anderson, B. J., C. L. Johnson, H. Korth, M. E. Purucker, R. M. Winslow, J. A. Slavin, S. C. Solomon, R. L. McNutt Jr., J. M. Raines, and T. H. Zurbuchen (2011), The global magnetic field of Mercury from MESSENGER orbital observations, *Science*, *333*(6051), 1859–1862.

Anderson, O. L. (2002), The power balance at the core-mantle boundary, *Phys. Earth Planet. Inter.*, *131*(1), 1–17.

Andrault, D., N. Bolfan-Casanova, G. Lo Nigro, M. A. Bouhifd, G. Garbarino, and M. Mezouar (2011), Solidus and liquidus profiles of chondritic mantle: Implication for melting of the Earth across its history, *Earth Planet. Sci. Lett.*, *304*, 251–259.

Anzellini, S., A. Dewaele, M. Mezouar, P. Loubeyre, and G. Morard (2013), Melting of iron at Earth's inner core boundary based on fast X-ray diffraction, *Science*, *340*, 464–467.

Aubert, J., H. Amit, G. Hulot, and P. Olson (2008), Thermochemical flows couple the Earth's inner core growth to mantle heterogeneity, *Nature*, *454*(7205), 758–761.

Aubert, J., S. Labrosse, and C. Poitou (2009), Modeling the paleo-evolution of the geodynamo, *Geophys. J. Int.*, *179*, 1414–1428.

Aubert, J., C. C. Finlay, and A. Fournier (2013), Bottom-up control of geomagnetic secular variation by the Earth's inner core, *Nature*, *502*(7470), 219–223.

Becker, T. W., C. P. Conrad, B. Buffett, and R. D. Müller (2009), Past and present seafloor age distributions and the temporal evolution of plate tectonic heat transport, *Earth Planet. Sci. Lett.*, *278*, 233–242.

Bercovici, D., and Y. Ricard (2014), Plate tectonics, damage and inheritance, *Nature*, *508*(7497), 513–516.

Besse, J., and V. Courtillot (2002), Apparent and true polar wander and the geometry of the geomagnetic field over the last 200 Myr, *J. Geophys. Res.*, *107*(B11), 2300, doi:10.1029/2000JB000050.

Bi, Y., H. Tan, and F. Jing (2002), Electrical conductivity of iron under shock compression up to 200 GPa, *J. Phys. Condens. Matter*, *14*(44), 10,849–10,854.

Biggin, A., B. Steinberger, J. Aubert, N. Suttie, R. Holme, T. H. Torsvik, D. G. van der Meer, and D. J. J. van Hinsbergen (2012), Possible links between long-term geomagnetic variations and whole-mantle convection processes, *Nat. Geosci.*, *5*, 526–533.

Biggin, A., E. Piispa, L. Pesonen, R. Holme, G. Paterson, T. Veikkolainen, and L. Tauxe (2015), Palaeomagnetic field intensity variations suggest mesoproterozoic inner-core nucleation, *Nature*, *526*(7572), 245–248.

Bloxham, J., D. Gubbins, and A. Jackson (1989), Geomagnetic secular variation, *Philos. Trans. R. Soc. London A*, *329*(1606), 415–502.

Bower, D. J., M. Gurnis, and M. Seton (2013), Lower mantle structure from paleogeographically constrained dynamic Earth models, *Geochem. Geophys. Geosyst.*, *14*, 44–63, doi:10.1029/2012GC004267.

Brandon, A. D., and R. J. Walker (2005), The debate over core-mantle interaction, *Earth Planet. Sci. Lett.*, *232*, 211–225.

Buffett, B. A. (1992), Constraints on magnetic energy and mantle conductivity from the forced nutations of the Earth, *J. Geophys. Res.*, *97*, 19,581–19,597.

Buffett, B. A. (2003), The thermal state of Earth's core, *Science*, *299*(5613), 1675–1677.

Buffett, B. A. (2007), A bound on heat flow below a double crossing of the perovskite-postperovskite phase transition, *Geophys. Res. Lett.*, *34*, L17302, doi:10.1029/2007GL030930.

Buffett, B. A. (2014), Geomagnetic fluctuations reveal stable stratification at the top of the Earth's core, *Nature*, *507*(7493), 484–487.

Buffett, B. A., H. E. Huppert, J. R. Lister, and A. W. Woods (1992), Analytical model for solidification of the Earth's Core, *Nature*, *356*(6367), 329–331.

Buffett, B. A., H. E. Huppert, J. R. Lister, and A. W. Woods (1996), On the thermal evolution of the Earth's core, *J. Geophys. Res.*, *101*, 7989–8006.

Buffett, B. A., E. J. Garnero, and R. Jeanloz (2000), Sediments at the top of the core, *Science*, *290*, 1338–1342.

Bull, A. L., M. Domeier, and T. H. Torsvik (2014), The effect of plate motion history on the longevity of deep mantle heterogeneities, *Earth Planet. Sci. Lett.*, *401*, 172–182.

Bullard, E. C. (1949), The magnetic field within the Earth, *Proc. R. Soc. London, Ser. A*, *197*, 433–453.

Bunge, H. P., C. R. Hagelberg, and B. J. Travis (2003), Mantle circulation models with variational data assimilation: Inferring past mantle flow and structure from plate motion histories and seismic tomography, *Geophys. J. Int.*, *152*, 280–301.

Burke, K. (2011), Plate tectonics, the Wilson cycle, and mantle plumes: Geodynamics from the Top, *Annu. Rev. Earth Planet. Sci.*, *39*, 1–29.

Burke, K., and T. H. Torsvik (2004), Derivation of large igneous provinces of the past 200 million years from long-term heterogeneities in the deep mantle, *Earth Planet. Sci. Lett.*, *227*(3-4), 531–538.

Burke, K., B. Steinberger, T. H. Torsvik, and M. A. Smethhurst (2008), Plume generation zones at the margins of large low shear velocity provinces on the core-mantle boundary, *Earth Planet. Sci. Lett.*, *265*, 49–60.
Calkins, M. A., J. Noir, J. D. Eldredge, and J. Aurnou (2012), The effects of boundary topography on convection in Earth's core, *Geophys. J. Int.*, *189*, 799–814.
Christensen, U., and J. Aubert (2006), Scaling properties of convection-driven dynamos in rotating spherical shells and application to planetary magnetic fields, *Geophys. J. Int.*, *166*, 97–114.
Christensen, U., P. Olson, and G. A. Glatzmaier (1998), A dynamo model interpretation of geomagnetic field structures, *Geophys. Res. Lett.*, *25*, 1565–1568.
Coe, R. S., S. Grommè, and E. A. Mankinen (1978), Geomagnetic paleointensities from radiocarbon-dated lava flows on Hawaii and the question of the Pacific nondipole low, *J. Geophys. Res.*, *83*, 1740–1756.
Cognè, J. P., and E. Humler (2004), Temporal variations of oceanic spreading and crustal production rates during the last 180 My, *Earth Planet. Sci. Lett.*, *227*, 427–439.
Courtillot, V. E., and P. R. Renne (2003), On the ages of flood basalt events, *C. R. Geosci.*, *335*(1), 113–140.
Davies, C. J. (2015), Cooling history of Earth's core with high thermal conductivity, *Phys. Earth Planet. Inter.*, *247*, 67–79.
de Koker, N., G. Steinle-Neumann, and V. Vlcek (2012), Electrical resistivity and thermal conductivity of liquid Fe alloys at high P and T, and heat flux in Earth's core, *Proc. Natl. Acad. Sci. U. S. A.*, *109*, 4070–4073.
Deleplace, B., and P. Cardin (2006), Viscomagnetic torque at the core mantle boundary, *Geophys. J. Int.*, *167*, 557–566.
de Wijs, G. A., G. Kresse, L. Vocadlo, D. Dobson, D. Alfé, M. J. Gillan, and G. D. Price (1998), The viscosity of liquid iron at the physical conditions of the Earth's core, *Nature*, *392*, 805–807.
Domeier, M., and T. H. Torsvik (2014), Plate tectonics in the late Paleozoic, *Geosci. Frontiers*, *5*(3), 303–350.
Driscoll, P., and D. Bercovici (2014), On the thermal and magnetic histories of Earth and Venus: Influences of melting, radioactivity, and conductivity, *Phys. Earth Planet. Inter.*, *236*, 36–51.
Driscoll, P. E., and D. A. Evans (2016), Frequency of Proterozoic geomagnetic superchrons, *Earth Planet. Sci. Lett.*, *437*, 9–14.
Dumberry, M., and J. Bloxham (2004), Variations in the Earth's gravity field caused by torsional oscillations in the core, *Geophys. J. Int.*, *159*, 417–434.
Dziewonski, A. M., V. Lekic, and B. A. Romanowicz (2010), Mantle anchor structure: An argument for bottom up tectonics, *Earth Planet. Sci. Lett.*, *299*, 69–79.
French, S. W., and B. A. Romanowicz (2015), Broad plumes rooted at the base of the Earth's mantle beneath major hotspots, *Nature*, *525*, 95–99.
Gillet, N., D. Jault, E. Canet, and A. Fournier (2010), Fast torsional waves and strong magnetic field within the Earth's core, *Nature*, *465*, 74–77.
Gomi, H., and K. Hirose (2015), Electrical resistivity and thermal conductivity of hcp Fe-Ni alloys under high pressure: Implications for thermal convection in the Earth's core, *Phys. Earth Planet. Inter.*, *247*, 2–10.
Gomi, H., K. Ohta, K. Hirose, S. Labrosse, R. Caracas, M. J. Verstraete, and J. W. Hernlund (2013), The high conductivity of iron and thermal evolution of the Earth's core, *Phys. Earth Planet. Inter.*, *224*, 88–103.
Gubbins, D., and C. J. Davies (2013), The stratified layer at the core-mantle boundary caused by baro-diffusion of oxygen, sulphur and silicon, *Phys. Earth Planet. Inter.*, *215*, 21–28.
Gubbins, D., T. G. Masters, and J. A. Jacobs (1979), Thermal evolution of the Earth's core, *Geophys. J. R. Astron. Soc.*, *59*(1), 57–99.
Gubbins, D., D. Alfé, G. Masters, G. D. Price, and M. Gillan (2004), Gross thermodynamics of two-component core convection, *Geophys. J. Int.*, *157*, 1407–1414.
Gubbins, D., D. Alfé, C. Davies, and M. Pozzo (2015), On core convection and the geodynamo: Effects of high electrical and thermal conductivity, *Phys. Earth Planet. Inter.*, *247*, 56–64.
Helffrich, G., and S. Kaneshima (2010), Outer-core compositional stratification from observed core wave speed profiles, *Nature*, *468*, 807–809.
Hernlund, J. W., C. Thomas, and P. J. Tackley (2005), A doubling of the post-perovskite phase boundary and structure of the Earth's lowermost mantle, *Nature*, *434*(7035), 882–886.
Herring, T. A., P. M. Mathews, and B. A. Buffett (2002), Modeling of nutation and precession: Very long baseline results, *J. Geophys. Res.*, *107*(B4), 2069, doi:10.1029/2001JB000165.
Hirose, K., S. Labrosse, and J. Hernlund (2013), Compositional state of Earth's core, *Annu. Rev. Earth Planet. Sci.*, *41*, 657–691.
Jault, D., and J.-L. LeMouel (1989), The topographic torque associated with tangentially geostrophic motion at the core surface and inferences on the flow inside the core, *Geophys. Astrophys. Fluid Dyn.*, *48*, 273–296.
Jaupart, C., S. Labrosse, and J. C. Mareschal (2007), Temperatures, heat and energy in the mantle of the Earth, in *Treatise on Geophysics*, vol. 7, edited by D. Bercovici, pp. 90–164, Elsevier Sci., Amsterdam.
Jeanloz, R. (1990), The nature of the Earth's core, *Annu. Rev. Earth Planet. Sci.*, *18*, 357–386.
Keeler, R. N. (1971), Electrical conductivity of condensed media at high pressures, in *Physics of High Energy Density*, vol. 48, edited by P. Caldirola and H. Knoepel, pp. 106–125, Academic, N. Y.
Korenaga, J. (2008), Urey ratio and the structure and evolution of Earth's mantle, *Rev. Geophys.*, *46*, RG2007, doi:10.1029/2007RG000241.
Labrosse, S. (2002), Hotspots, mantle plumes and core heat loss, *Earth Planet. Sci. Lett.*, *199*(1–2), 147–156.
Labrosse, S. (2003), Thermal and magnetic evolution of the Earth's core, *Phys. Earth Planet. Inter.*, *140*, 127–143.
Labrosse, S. (2015), Thermal evolution of the core with a high 302 thermal conductivity, *Phys. Earth Planet. Inter.*, *247*, 36–55.
Larson, R. L., and P., Olson (1991), Mantle plumes control magnetic reversal frequency, *Earth Planet. Sci. Lett.*, *107*(3), 437–447.
Larson, R. L. (1991), Latest pulse of Earth - evidence for a mid Cretaceous superplume, *Geology*, *19*, 547–550.
Lay, T., J. Hernlund, E. J. Garnero, and M. S. Thorne (2006), A post-perovskite lens and D'' heat flux beneath the central Pacific, *Science*, *314*, 1272–1276.
Lay, T., J. Hernlund, and B. A. Buffett (2008), Core-mantle boundary heat flow, *Nat. Geosci.*, *1*, 25–32.
Li, M., B. Black, S. Zhong, M. Manga, M. L. Rudolph, and P. Olson (2015), Quantifying melt production and degassing rate at mid-ocean ridges from global mantle convection models with plate motion history, Abstract presented at 2015 Fall Meeting, AGU, San Francisco, Calif.
Lithgow-Bertelloni, C., and M. A. Richards (1998), Dynamics of Cenozoic and Mesozoic plate motion, *Rev. Geophys.*, *36*, 27–78.
Lister, J. R., and B. A. Buffett (1995), The strength and efficiency of thermal and compositional convection in the geodynamo, *Phys. Earth Planet. Inter.*, *91*(1), 17–30.
Loper, D. E. (1978), The gravitationally powered dynamo, *Geophys. J. R. Astron. Soc.*, *54*(2), 389–404.
Loyd, S. J., T. W. Becker, C. P. Conrad, C. Lithgow-Bertelloni, and F. Corsetti (2007), Time variability in Cenozoic reconstructions of mantle heat flow: Plate tectonic cycles and implications for Earth's thermal evolution, Proc. *Natl. Acad. Sci. U. S. A.*, *104*, 14,266–14,271.

Matassov, G. (1977), The electrical conductivity of iron-silicon alloys at high pressures and the earth's core, PhD dissertation, Univ. of Calif., Davis.
Matsui, H., et al. (2016), Performance benchmarks for a next generation numerical dynamo model, *Geochem. Geophys. Geosyst.*, doi: 10.1002/2015GC006159, in press.
McFadden, M., and C. J. Johnson (2015), The time averaged field and secular variation, in *Treatise on Geophysics*, vol. 5, 2nd ed., edited by G. Schubert, chap. 11, Elsevier, Oxford, U. K.
McNamara, A. K., and S. J. Zhong (2004), Thermochemical structures within a spherical mantle: Superplumes or piles?, *J. Geophys. Res.*, *109*, B07402, doi:10.1029/2003JB002847.
McNamara, A. K., and S. J. Zhong (2005), Thermochemical structures beneath Africa and the Pacific Ocean, *Nature*, *437*, 1136–1139.
Monnereau, M., and D. A. Yuen (2010), Seismic imaging of the D'' and constraints on the core heat flux, *Phys. Earth Planet. Inter.*, *180*(3–4), 258–270.
Mound, J. E., and B. A. Buffett (2005a), Mechanisms of core-mantle angular momentum exchange and the observed spectral properties of torsional oscillations, *J. Geophys. Res.*, *110*, B08103, doi:10.1029/2004JB0035555.
Mound, J. E., and B. A. Buffett (2005b), Detection of a gravitational oscillation in length of day, *Earth Planet. Sci. Lett.*, *243*, 383–389.
Müller, R. D., C. Gaina, and W. R. Roest (2008), Age, spreading rates, and spreading asymmetry of the world's ocean crust, *Geochem. Geophys. Geosyst.*, *9*, Q04006, doi:10.1029/2007GC001743.
Nakagawa, T., and P. J. Tackley (2005), Deep mantle heat flow and thermal evolution of the Earth's core in thermochemical multiphase models of mantle convection, *Geochem. Geophys. Geosyst.*, *6*, Q08003, doi:10.1029/2005GC000967.
Nakagawa, T., and P. J. Tackley (2008), Lateral variations in CMB heat flux and deep mantle seismic velocity caused by a thermal-chemical-phase boundary layer in 3D spherical convection, *Earth Planet. Sci. Lett.*, *271*, 348–358.
Nakagawa, T., and P. J. Tackley (2010), Influence of initial CMB temperature and other parameters on the thermal evolution of Earth's core resulting from thermochemical spherical mantle convection, *Geochem. Geophys. Geosyst.*, *11*, Q06001, doi:10.1029/2010GC003031.
Nakagawa, T., and P. J. Tackley (2011), Effects of low-viscosity post-perovskite on thermochemical mantle convection in a 3D spherical shell, *Geophys. Res. Lett.*, *38* L04309, doi:10.1029/2010GL046494.
Nakagawa, T., and P. J. Tackley (2013), Implications of high core thermal conductivity on Earth's coupled mantle and core evolution, *Geophys. Res. Lett.*, *40*, 2652–2656, doi:10.1002/grl.50574.
Nakagawa, T., and P. J. Tackley (2015), Influence of combined primordial layering and recycled MORB on the coupled thermal evolution of Earth's mantle and core, *Geochem. Geophys. Geosyst.*, *15*, 619–633, doi:10.1002/2013GC005128.
Nakajima, M., and D. J. Stevenson (2015), Melting and mixing states of the Earth's mantle after the moon-forming impact, Earth *Planet. Sci. Lett.*, *427*, 286–295.
Nimmo, F. (2015), Energetics of the core, in *Treatise on Geophysics*, vol. 8, 2nd ed., edited by G. Schubert, chap. 2, Elsevier, Oxford, U. K.
Ogawa, M. (2016), Evolution of the interior of Mercury influenced by coupled magmatism-mantle convection system and heat flux from the core, *J. Geophys. Res. Planets*, *121*, 118–136, doi:10.1002/2015JE004832.
Ohta, K., T. Yagi, N. Taketoshi, K. Hirose, T. Komabayashi, T. Baba, Y. Ohishi, and J. Hernlund (2012), Lattice conductivity of $MgSiO_3$ perovskite and post-perovskite at the core-mantle boundary, *Earth Planet. Sci. Lett.*, *349-350*, 109–115.
Olson, P., and J. Aurnou (1999), A polar vortex in the Earth's core, *Nature*, *402*(6758), 170–173.
Olson, P., R. Deguen, L. A. Hinnov, and S. Zhong (2013), Controls on geomagnetic reversals and core evolution by mantle convection in the Phanerozoic, *Phys. Earth Planet. Inter.*, *214*, 87–103.
Olson, P., R. Deguen, M. L. Rudolph, and S. Zhong (2015), Core evolution driven by mantle global circulation, *Phys. Earth Planet. Inter.*, *243*, 44–55.
O'Rourke, J. G., and D. J. Stevenson (2016), Powering Earth's dynamo with magnesium precipitation from the core, *Nature*, *529*(7586), 387–389.
Paulson, A., S. Zhong, and J. Wahr (2007), Inference of mantle viscosity from GRACE and relative sea level data, *Geophys. J. Inter.*, *171*(2), 497–508.
Phillips, B. R., and P. H. Bunge (2005), Heterogeneity and time dependence in 3D spherical mantle convection models with continental drift, *Earth Planet. Sci. Lett.*, *233*, 121–135.
Pozzo, M., C. Davies, D. Gubbins, and D. Alfé (2012), Thermal and electrical conductivity of iron at Earth's core conditions, *Nature*, *485*, 355–358.
Pozzo, M., C. Davies, D. Gubbins, and D. Alfé (2014), Thermal and electrical conductivity of solid iron and iron-silicon mixtures at earth's core conditions, Earth *Planet. Sci. Lett.*, *393*, 159–164.
Roberts, J., R. Lillis, and M. Manga (2009), Giant impacts on early mars and the cessation of the Martian dynamo, *J. Geophys. Res.*, *114*, E04009, pp. 123–157, N. Y., doi:10.1029/2008JE003287.
Romanowicz, B., and Y. Gung (2002), Superplumes from the core-mantle boundary to the lithosphere: Implications for heat flux, *Science*, *296*, 513–516.
Rubie, D., D. J. Frost, U. Mann, Y. Asahara, F. Nimmo, K. Tsuno, P. Kegler, A. Holzheid, and H. Palm (2011), Heterogeneous accretion, composition and core-mantle differentiation of the Earth, Earth *Planet. Sci. Lett.*, *301*, 31–42.
Rudolph, M., and S. J. Zhong (2014), History and dynamics of net rotation of the mantle and lithosphere, *Geochem. Geophys. Geosyst.*, *15*, 3645–3657, doi:10.1002/2014GC005457.
Scotese, C. R. (1997), *Continental Drift*, 7th ed., 79 pp., PALEOMAP Project, Arlington, Tex.
Scotese, C. R. (2001), Atlas of Earth history, *PALEOMAP Progress Rep. 90-0497*, Dep. of Geol., Univ. of Tex. at Arlington, Arlington.
Seagle, C. T., E. Cottrell, Y. Fei, D. R. Hummer, and V. B. Prakapenka (2013), Electrical and thermal transport properties of iron and iron-silicon alloy at high pressure, *Geophys. Res. Lett.*, *40*, 5377–5381, doi:10.1002/2013GL057930.
Selkin, P. A., and L. Tauxe (2000), Long-term variations in palaeointensity, *Philos. Trans. R. Soc. London A*, *358*(1768), 1065–1088.
Seton, M., et al. (2012), Global continental and ocean basin reconstructions since 200 Ma, *Earth Sci. Rev.*, *113*, 212–270.
Shirey, S. B., and S. H. Richardson (2011), Start of the Wilson cycle at 3 Ga shown by diamonds from subcontinental mantle, *Science*, *333*(6041), 434–436.
Stacey, F. D. (1977), A thermal model of the Earth, *Phys. Earth Planet. Inter.*, *15*(4), 341–348.
Stacey, F. D., and O. L. Anderson (2001), Electrical and thermal conductivities of Fe-Ni-Si alloy under core conditions, *Phys. Earth Planet. Inter.*, *124*(3), 153–162.
Stacey, F. D., and D. E. Loper (1983), The thermal boundary layer interpretation of D'' and its role as a plume source, *Phys. Earth Planet. Inter.*, *33*(1), 45–55.
Stacey, F. D., and D. E. Loper (1984), Thermal histories of the core and mantle, *Phys. Earth Planet. Inter.*, *36*(2), 99–115.

Stacey, F. D., and D. E. Loper (2007), A revised estimate of the conductivity of iron alloy at high pressure and implications for the core energy balance, *Phys. Earth Planet. Inter.*, *161*(1–2), 13–18, doi:10.1016/j.pepi.2006.12.001.

Steinberger, B., and T. H. Torsvik (2008), Absolute plate motions and true polar wander in the absence of hotspot tracks, *Nature*, *452*, 620–624.

Tang, V., L. Zhao, and S. Hung (2015), Seismological evidence for a non-monotonic velocity gradient in the topmost outer core, *Sci. Rep.*, *5*, 8613.

Tarduno, J. A., R. D. Cottrell, M. K. Watkeys, A. Hofmann, P. V. Doubrovine, E. E. Mamajek, D. D. Liu, D. G. Sibeck, L. P. Neukirch, and Y Usui (2010), Geodynamo, solar wind and magnetopause 3.4 to 3.45 billion years ago, *Science*, *327*, 1238–1240.

Tarduno, J. A., R. D. Cottrell, W. J. Davis, F. Nimmo, and R. K. Bono (2015a), A Hadean to Paleoarchean geodynamo recorded by single zircon crystals, *Science*, *349*(6247), 521–524.

Tarduno, J. A., M. K. Watkeys, T. N. Huffman, R. D. Cottrell, E. G. Blackman, A. Wendt, C. A. Scribner, and C. L. Wagner (2015b), Antiquity of the South Atlantic anomaly and evidence for top-down control on the geodynamo, *Nat. Commun.*, *6*, 7865.

Tateno, S., K. Hirose, N. Sata, and Y. Ohishi (2009), Determination of post-perovskite phase transition boundary up to 4400 K and implications for thermal structure in D'' layer, *Earth Planet. Sci. Lett.*, *277*(1-2), 130–136, doi:10.1016/j.epsl.2008.10.004.

Tauxe, L., and T. Yamazaki (2007), Paleointensities, in *Treatise on Geophysics, vol. 5, Geomagnetism*, chap. 13, pp. 509–563, Elsevier, Amsterdam.

Tilgner, A. (2015), Rotational dynamics of the core, in *Treatise on Geophysics, vol. 8, Core Dynamics*, 2nd ed., edited by P. Olson, chap. 8, Elsevier, Amsterdam.

Torsvik, T. H., and R. M. Cocks (2004), Earth geography from 400 to 250 Ma: A palaeomagnetic, faunal and facies review, *J. Geol. Soc. London*, *161*, 555–572.

Torsvik, T. H., M. A. Smethhurst, K. Burke, and B. Steinberger (2006), Large igneous provinces generated from the margins of the large low-velocity provinces in the deep mantle, *Geophys. J. Int.*, *167*, 1447–1460.

Torsvik, T. H., M. A. Smethurst, K. Burke and B. Steinberger (2008), Long term stability in deep mantle structure: Evidence from the ~300 Ma Skagerrak-Centered Large Igneous Province (the SCLIP), *Earth Planet. Sci. Lett.*, *267*(3), 444–452.

Van der Hilst, R., M. V. de Hoop, P. Wang, S.-H. Shim, P. Ma, and L. Tenorio (2007), Seismostratigraphy and thermal structure of Earth's core-mantle boundary region, *Science*, *315*, 1379–1381.

Watanabe, K., E. Ohtani, S. Kamada, T. Sakamaki, M. Miyahara, and Y. Ito (2014), The abundance of potassium in the Earth's core, *Phys. Earth Planet. Inter.*, *237*, 65–72.

Whaler, K. (1980), Does the whole of the earth's core convect?, *Nature*, *287*, 528–530.

Wu, B., P. Olson, and P. Driscoll (2011), A statistical boundary layer model for the mantle D''-region, *J. Geophys. Res.*, *116*, B12112, doi: 10.1029/2011JB008511.

Zhang, N., and S. J. Zhong (2011), Heat fluxes at the Earth's surface and core-mantle boundary since Pangea formation and their implications for the geomagnetic superchrons, *Earth Planet. Sci. Lett.*, *306*, 205–216.

Zhang, N., S. J. Zhong, W. Leng, and Z. X. Li (2010), A model for the evolution of the Earth's mantle structure since the Early Paleozoic, *J. Geophys. Res.*, *115*, B06401, doi:10.1029/2009JB006896.

Zhang, P., R. E. Cohen, and K. Haule (2015), Effects of electron correlations on transport properties of iron at Earth's core conditions, *Nature*, *517*, 605–607.

Zhong, S. J. (2006), Constraints on thermochemical convection of the mantle from plume heat flux, plume excess temperature, and upper mantle temperature, *J. Geophys. Res.*, *111*, B04409, doi:10.1029/2005JB003972.

Zhong, S. J., and M. L. Rudolph (2015), On the temporal evolution of long-wavelength mantle structure of the Earth since the Early Paleozoic, *Geochem. Geophys. Geosyst.*, *16*, 1599–1615, doi:10.1002/2015GC005782.